A FINITE ELEMENT ANALYSIS OF A SINGLE LAP SHEAR ADHESIVE JOINT WITH AND WITHOUT AN EDGE CRACK.

Thomas Holm Christensen

A FINITE ELEMENT ANALYSIS OF A SINGLE LAP SHEAR ADHESIVE JOINT WITH AND WITHOUT AN EDGE CRACK

by

THOMAS HOLM CHRISTENSEN

S.B., University of California, Berkeley
1970

Submitted in partial fulfillment of the requirements
for the simultaneous award of the degrees of

MASTER OF SCIENCE, MATERIALS SCIENCE AND ENGINEERING

and

MASTER OF SCIENCE, OCEAN ENGINEERING

at the

MASSACHUSETTS INSTITUTE OF TECHNOLOGY

February, 1976

ABSTRACT

A FINITE ELEMENT ANALYSIS OF A SINGLE LAP SHEAR ADHESIVE JOINT WITH AND WITHOUT AN EDGE CRACK

by

THOMAS HOLM CHRISTENSEN

Submitted to the Department of Materials Science and Engineering and to the Department of Ocean Engineering on January 21, 1976 in partial fulfillment of the requirements for the degrees of Master of Science in Materials Science and Engineering, and Master of Science in Ocean Engineering.

The single lap shear adhesive joint is analyzed both with and without a short edge crack using the finite element method. The method employed is more accurate than previous numerical solutions due to the use of a more accurate element (assumed stress hybrid element and crack tip superelement) and a finer mesh than previously applied. The results of the analysis without a crack shows a large variation in stress across the adhesive not previously reported. The results also show previous determinations of stress at the end of lap to be conservative. The results also specifically address longitudinal stress in the adherend which have been discussed experimentally, but not published numerically. The analysis of the single lap joint with a short edge crack represents the first application of the general nine node singular hybrid stress "super element" to a real problem. Results indicate a power law relation between stress intensity factors k_I and k_{II}, and the modulus ratio. It is shown that k_{II} is not only of the same magnitude as k_I, but actually slightly larger, which indicates that a failure mechanism must be combined mode. The analysis indicates no difference between the uncracked joint and the cracked one (crack length 2.5 adhesive thicknesses) at distances greater than ten adhesive thicknesses away from the crack tip.

Thesis Supervisor: Professor F. J. McGarry
Title: Professor of Materials Science and Engineering
Professor of Civil Engineering
Thesis Supervisor: Professor Norman Jones
Title: Associate Professor of Ocean Engineering

Table of Contents

List of Illustrations

List of Illustrations Continued

List of Tables

ACKNOWLEDGEMENTS

The author wishes to express his deep appreciation to Dr. Su Su Wang for his constant advice and continuous guidance and assistance throughout the research reported herein. He is also grateful to Dr. John Mandell and Professor F.J. McGarry for their valuable suggestions and constructive criticism during the course of the research. The digital computations were carried out at the M.I.T. Information Processing Center with funds provided by the American Cyanamid Company. The author wishes to thank his wife, Marilyn, for proof reading and typing the manuscript.

Section I: Introduction

This research was undertaken to investigate the stress distribution in a single lap shear adhesive bonded joint. The analysis of the problem was done using the finite element method (FEM). The intent was to determine the stress field, in the configuration shown in Figure 1, both with no crack present and with a single short edge crack. In particular, this research investigates the variation in stress across the adhesive layer without a crack, and then analyzes the changes in the solution when a short edge crack is introduced. The short crack (2.5 adhesive thicknesses) was chosen so that the constraint conditions which were found to be stable (i.e., no kinematic modes) for the uncracked case would still be appropriate for the joint with a short crack. The crack length used herein idealizes a shrinkage or residual stress induced edge crack.

To fully investigate the lap shear adhesive bonded joint would require a vast parametric study which systematically investigates the effect of geometric variables,(e.g., overlap length, adhesive thickness, adherend thickness, adherend shape in the overlap region, and the adhesive shape at the end of lap, crack length, and location of crack(s)), as well as material properties, (e.g., Young's modulus ratio for isotropic adherend and adhesive, different Poisson ratios for adherend and adhesive and anisotropic materials.) This research concentrates on the effect of the Young's modulus ratio over a range of one to one thousand with other variables held constant and over varied adhesive thicknesses with other variables held constant.

Section II is a brief critical review of the literature on adhesive bonded joints as it relates to this research. Section III is a brief discussion of the FEM. Section IV is a discussion of the singular crack tip element or super element used in the research reported herein in the analysis

of the joints with short edge cracks. Section V is a presentation of the results and discussion of this research on uncracked adhesive bonded lap shear joints. Section VI is a presentation of the results for an adhesive bonded lap shear joint with a single edge crack and a comparison with the uncracked case as presented in Section V. Section VII is a summary of the results of the previous sections and a presentation of the conclusions to be drawn from this research. Section VIII contains suggestions for further work to be undertaken on lap shear joints, using the FEM.

Section II: Literature Review

The literature on adhesive bonded joints can be divided into three broad categories. First, there are the "classical" solutions which, more or less, attempt a closed form solution after making simplifying assumptions. Second, there are the numerical techniques of finite differences and the FEM. Third, there are the experimental investigations of joint strength, fracture mechanisms, and rough stress distribution approximation.

i. Classical Solutions

Goland and Reissner [1] were the first to include the effects of bending with those of differential straining in their solution to the adhesive bonded lap joint in tension. Their solution assumes the adhesive layer to be very thin relative to other typical dimensions in the problem and, therefore, ignores this thickness in calculating the stresses. The solution assumes linear normal stress and parabolic shear distribution, thereby reducing the problem to that of a cylindrically bent plate or thin beam theory. The primary weakness in their solution is that it

is assumed that the stresses do not vary across the adhesive thickness. The error in assuming a constant state of stress will be shown in Section V, when the result of this research is presented. The Goland and Reissner approximations, however, have been widely used as a measure of the validity of experimental studies, such as, by the U.S. Forest Service [2]. Although modifications have been made to the Goland and Reissner stress equations, the shape of the stress curves are similar. For this reason, the Goland and Reissner equations are included as Appendix I, and a comparison of their solution with the current research is presented for a typical geometry in Figure 2 (tearing stress) and Figure 3 (shear stress).

Cornell [3] used Goland and Reissner's work as a basis and, his solution has the same error in that he also assumes a constant state of stress across the adhesive layer. Cornell treats the adherends as independent beams connected by an infinite number of shear and tension springs. The research reported herein finds that Cornell's solution to the resulting differential equations greatly underestimates the longitudinal stress in the adherend. High longitudinal stress is due to the localized bending effect near the end of the lap. This has been shown to exist experimentally by Wang, *et al.* [4], and others, and to be sufficiently high to cause plastic flow and even failure in the adherend.

Not all of the "classical" solutions are as old as Goland and Reissner's work and Cornell's work. Schijve [5] has done a thin beam analysis of lap shear problems to determine the effect of clamping conditions and permanent deformation on secondary bending. Schijve, as in previously reported classical works, assumes a thin adhesive layer with a constant stress state across its thickness. His work indicates that permanent set, or local plastic deformation, has a greater effect than clamping conditions on secondary bending (i.e., stress at the end of lap).

This again points to the importance of determining the longitudinal stress in the adherend, however, very few papers discuss longitudinal stresses at all.

Chang and Muki [6] have solved the lap shear problem by reducing the problem to a pair of Fredholm integral equations of the second kind, which they then solve for bond line stresses and stress concentration factors at the end of the bonded region. The solution is dependent on the angle of rotation of the joint, which is determined by the Goland and Reissner solution. Chang and Muki also assume an infinitessimally thin adhesive layer and traction and displacement vectors continuous across the bond. As would be expected with the same basic assumptions as Goland and Reissner, the results are similar including a constant state of stress across the bond.

Srinivas [7] has divided the lap into regions where the adhesive layer is treated as an infinite number of elastic tension and shear springs. This is similar to the method reported by Cornell. Srinivas, however, does not use thin beam theory. Instead, he expands the longitudinal displacement (u) and the transverse displacement (w) up to the second order in the transverse coordinate (z), where the undetermined coefficients are functions of the longitudinal coordinate (x) only. These assumed displacements are then used with the governing equations of elasticity with appropriate boundary conditions within each region to obtain a solution for strains, which, in turn, determines stresses through the stress-strain relations. The formulation is sufficiently involved that a digital computer is required to solve the resulting linear equations. Because the displacement functions are limited to the second order, this solution is no better than a finite element formulation with a single hybrid element (discussed in Section III) or a single eight node displacement model quadrilateral element (found in introductory

texts on FEM [8,9]), across the adherend thickness with similar boundary conditions at the bond. Either of the latter would be considered unreasonably coarse, yet both are of the same degree of accuracy as that reported by Srinivas. There are no "classical" treatments of the lap shear adhesive bonded joint with a crack. This is not surprising since the classical solutions assume infinitessimal adhesive thickness and, therefore, cannot address a crack in a region which is not directly treated in the formulation of the problem.

ii. Numerical Techniques

Wooley and Carver [10] used the FEM to analyze the adhesive bonded lap shear joint. Their work has several basic flaws. First, the physical geometry of the adhesive bonded lap joint, (i.e., width much greater than overlap length or thickness) makes plane strain, as used by all previously mentioned investigators, appropriate, yet Wooley and Carver assume plane stress. Second, they use quadrilateral elements comprised of four triangular subelements which produce constant stress within each element, and less accurate results. This shortcoming could be reduced by a more imaginative use of mesh arrangement. Wooley and Carver use equal mesh spacing across the thickness and along the lap region which causes them to completely miss the very high stress concentration that exists at the end of lap for low adherend to adhesive modulus ratios due to the geometric and material discontinuities.

Harrison and Harrison [11] also apply the FEM to the lap shear joint, and likewise, their research has several flaws. First, and foremost, they assume a symmetry about the midplane of the bond which does not physically exist. They hypothesize that the real lap shear problem can be approximated by a linear combination of uniform displacement boundary conditions on the

bond line. None of the previous literature leads one to believe that this is a reasonable assumption. Second, their formulation neglects rotation and, therefore, could never predict incipient failure in the longitudinal direction due to adherend yielding. Third, and of less importance, they use all constant strain elements. This requires far more degrees of freedom and, therefore, computation time, than other elements discussed in Section III.

Pirvics [12] investigates the lap shear problem using a finite difference technique. The physical dimensions used in Pirvics' analysis appear to unduly restrict rotation of the system. That is to say, a fixed end condition is imposed on one adherend at a distance of only one inch from the joint. Also, an extremely short overlap length of 0.12 inch is used, well out of the normal commercially used range of 0.50-1.50 inches. The finite difference technique is inherently a slowly convergent method. The finite difference method also has great difficulty handling boundaries. A boundary requires a transformation of the actual shape so that method of images can approximate the real problems discontinuous shape at the boundary. Because of the concentration of stresses near a boundary in the physical problem, and the difficulty in treating boundary regions by the finite differences method noted above, the validity of using a finite differences technique is in question. Pirvics did not specifically state how the boundaries are to be treated.

Adams and Peppiatt [13] use the FEM in analyzing both single and double lap shear adhesive bonded joints. The only single lap shear configuration for which they present results has a square ended adhesive layer, which does not closely approximate a real single lap joint. In their analysis of double lap joints, they allow a fillet "spew" which is more realistic. That is to say, a real adhesive joint when put under some pressure at time of bonding will tend to

force some adhesive out of the lap region and form a fillet. Their analysis uses all constant strain triangular elements which have shortcomings as noted above. They do not address longitudinal stresses in the adherend, nor do they address a variation in stress across the adhesive layer.

Although some literature does exist on applications of the FEM to the adhesive bonded joint containing a crack, this problem and a discussion of this literature will be postponed to Section IV. None of the existing literature has used the singular hybrid stress element in the analysis of the lap shear problem containing a crack in the joint.

iii. Experimental Techniques

Experimental studies of lap joint configuration face the difficult task of trying to determine the stress distribution in a layer only five to ten thousandths of an inch thick. For this reason, most experimental studies use large models of the joint, and they apply the following modeling assumptions [14]:

a) Maintain the ratio of adherend thickness to adhesive thickness of the actual joint,

b) Maintain the same ratio of adherend shear modulus to adhesive shear modulus, or the general ratio of mechanical properties of adherend to adhesive, as in the actual joint,

c) Be wide enough to ensure a condition of plane strain in the plane of the adhesive,

d) Simulate a true adhesive bond between the adherend and adhesive. It is important to simulate the discontinuous nature of the mechanical properties at the adherend-adhesive interface.

The experimental literature on adhesive bonded lap joints can be broken into three

areas. First, there are photoelastic methods, such as those used by Cornell [3] to augment his theoretical work mentioned earlier, or Hahn [15], Kutscha [16] and others. Hahn's work presents two interesting conclusions, which have not been investigated in the literature. First, he notes inelastic behavior in the adherend, which, as previously discussed, has not been a focus of analytical efforts. Second, Hahn notes photoelastic behavior in the bond layer, particularly at the end of lap, which he interprets as a variation in stress across the adhesive layer. This is contrary to the assumption of infinitessimal thickness and continuous tractions from adherend to adherend as used in classical solution. The existing numerical techniques and analytical methods fail to show this variation across the bond line. This, then, is a major objective of the research reported herein.

The second area is the modeling of the real metal-adhesive-metal joint by rubbers of moduli appropriate to the modeling laws given above. Early work was done by NASA [17] and more recent work has been done by Adams, *et al*. [13,18]. The primary problem with both the photoelastic methods and rubber models is that only a qualitative idea of the stress distribution can be determined. Experimental models in general, and the rubber model in particular, have three additional drawbacks. First it has not been shown that the behavior of a one half inch or greater model adhesive layer is a good approximation to the real problem. Second, although the Young's modulus ratio or the shear modulus ratio are similar for the rubber model and the real problem, the Poisson ratios are greatly different. It has not been shown that this difference has a negligible effect on the results. Third, the rubber models are actually a five layer system with stiff-rubber/bond/foam-rubber/bond/stiff-rubber. Although the bond has similar properties, it is not clear that the five layer system closely approximates the real problem.

The final area of experimental work is that of destructive testing of actual adhesive bonded joints to determine allowable loading, mechanisms of fracture and other data required for safe design of joints. The Forest Products Laboratory Report [2] and research reported by Wang, *et al*. [4], Dukes and Bryant [19], and Grimes [20], are typical examples of destructive testing. Although significant observations can be made by direct experimentation, and the ultimate verification of any analytical method is by direct experimentation, this technique does not lead to understanding of the general case. That is to say, while Dukes and Bryant have established a relationship between adhesive thickness and reduced strength, it is known to be valid only in conjunction with the geometry and materials variables used. If an analytical or numerical method can be perfected which can predict failure from the computed stress field, and if it can be verified by destructive testing, then, and only then, will there be a high degree of confidence in the design of adhesive joints, without a costly testing program of actual geometries and materials. The research reported herein is hoped to be a step toward such a method.

Section III: Finite Element Method

The FEM is an extremely versatile and powerful application of the variational principles of mechanics by which a complex shaped continuum, such as the single lap shear joint, may be divided into a finite number of discrete elements. After dividing the continuum, displacement or stress fields, or both, are assumed within each element. The equations that result from the application of the appropriate variational principle are simultaneous linear algebraic equations which have generalized displacements, as unknowns to be determined [21].

In the research reported herein, three different elements were used (not counting the super element used at the crack tip of the cases that contained a crack. See Section IV. Two elements, an isoparametric triangular element, and an isoparametric quadrilateral element, are derived from the principle of minimum potential energy and are briefly outlined in section III.i. below. The remaining element is a rectangular hybrid element [22], based on the complimentary energy principle outlined in Section III.ii. below. The reason for using both the isoparametric quadrilateral element and the assumed stress hybrid rectangular element in the same problem is primarily one of accuracy. The rectangular hybrid element is as accurate as an eight node isoparametric quadrilateral element, but, having fewer degrees of freedom, is far more efficient with respect to computation time. The assumed stress hybrid method does not require a rectangular shape, however, if a rectangular shape is used, integrations along the boundary can be done before programming, which greatly increases efficiency. A general quadrilateral shape using the hybrid model requires numerical integration along each boundary segment which increases computation time. This problem was avoided in the research reported herein by arranging the mesh such that all general quadrilater shapes are only in less critical areas. Therefore, the more efficient (one nine point numerical integral vice eight five point numerical line integrals), but less accurate, isoparametric element was used in these areas, rather than a general quadrilateral assumed stress hybrid element.

This means that the entire problem reduces to the form

$$Kq = Q$$

where

K = the assembled global stiffness of the entire structure

q = generalized nodal displacements

Q = equivalent nodal forces

All three elements use a linear displacement interpolation function which assures compatibility along interelement boundaries. Therefore, it is appropriate and, as it will be shown, advantageous to use elements formulated from different variational principles.

i. Isoparametric Elements

The isoparametric elements are based on the assumption of a displacement field continuous over the entire solid. For this reason, they are often referred to as compatible models.

The formulation of the isoparametric triangular element or the isoparametric quadrilateral element can be found in any introductory texts on the FEM [8,9]. The isoparametric triangular element is first transformed to a parent element, as shown in Figure 4, in triangular or area coordinates such that

$$x = \sum_{i=1}^{3} P_i x_i \qquad y = \sum_{i=1}^{3} P_i y_i$$

where

$$P_1 = \xi_1$$
$$P_2 = \xi_2$$
$$P_3 = \xi_3$$

and

$$\xi_1 + \xi_2 + \xi_3 = 1$$

Similarly for the quadrilateral element, there is a transformation to a parent element, as shown in Figure 5, such that

$$x = \sum_{i=1}^{4} P_i x_i \qquad y = \sum_{i=1}^{4} P_i y_i$$

where

$$P_i = 1/4 (1 + \xi\xi_i) (1 + \eta\eta_i)$$

and

$$\sum_{i=1}^{4} P_i = 1$$

The principle of minimum potential energy for a plane elasticity problem may be stated as the vanishing of the variation of the total potential energy functional, π_p, which can be written for each element as

$$\pi_p = t \int_A (0.5\ \epsilon^T E\ \epsilon - u^T \bar{F})\, dA - \int_{s_\sigma} u^T \bar{T}\, ds$$

where

ϵ = strain vector

E = elastic constants

A = area of the element

$\bar{F}$ = prescribed body forces

$\bar{T}$ = prescribed surface traction

u = generalized displacements

s = boundary curve of element

s_σ = portion of s over which surface tractions are prescribed

t = thickness (assumed unity)

But u can be written as:

$$u = R\,q$$

where

q = unknown nodal displacements,

$R = \{R_1\ R_2 \ldots\ldots R_n\}$ n=3 for triangular element, n=4 for quadrilateral element

and

$$R_i = \begin{Bmatrix} P_i & 0 \\ 0 & P_i \end{Bmatrix}$$

therefore

$$\epsilon = D\,u$$

where

D is the differential operator $\begin{Bmatrix} (\partial/\partial x) & 0 \\ 0 & (\partial/\partial y) \\ (\partial/\partial y) & (\partial/\partial x) \end{Bmatrix}$

ϵ can be written

$$\epsilon = B\,q$$

where

$$B = \left\{ B_1 B_2 \ldots\ldots B_n \right\}$$

$$B_i = \begin{Bmatrix} (\partial P_i/\partial x) & 0 \\ 0 & (\partial P_i/\partial y) \\ (\partial P_i/\partial y) & (\partial P_i/\partial x) \end{Bmatrix}$$

defining the element stiffness matrix

$$k = \int_A B^T E B \, dA$$

and the equivalent nodal force

$$Q = \int_A R^T F \, dA + \int_{s\sigma} R^T T \, ds$$

The interpolation functions, however, are not in terms of x and y so a modification must be made to the integration to account for that fact. That is

$$k = \int_A B^T [J^{-1}]^T E B[J] \, dA$$

$$Q = \int_A R^T F \, dA + \int_{s\sigma} R^T T \, ds$$

where

$$dA = \left| \left| \frac{\partial (x,y)}{\partial (\xi_1, \xi_2)} \right| \right| d\xi_1 \, d\xi_2 \qquad \text{for the triangular element}$$

$$dA = \left| \left| \frac{\partial (x,y)}{\partial (\xi, \eta)} \right| \right| d\xi d\eta \qquad \text{for the quadrilateral element}$$

The integration of the triangular element simplifies significantly due to the property of integration in triangular coordinates

where

$$\frac{\partial(x,y)}{\partial(\xi_1,\xi_2)} = 2\dot{A}$$

and

A = Area of element

then

$$\int \xi_1^n \xi_2^m \xi_3^s \, dA = 2A \; \frac{m!\,n!\,s!}{(m+n+s+2)!}$$

The integration of the terms of k for the quadrilateral element are done numerically using a nine point Gaussian quadrature of the form (bi-linear three point quadrature)

$$\int_R f(x, y)\, dA = \sum_{i=1}^{3}\sum_{j=1}^{3} W_i W_j \, f(x_i,y_j)$$

where

W_i, W_j = weighting factors

$f(x_i,y_j)$ = value of the function $f(x,y)$ evaluated at (x_i,y_i)

ii. Rectangular Hybrid Element

The assumed stress hybrid model is based on the complementary energy principle. That principle can be written by the following functional for any element [22]:

$$\pi_c = t \int_R 0.5\, \sigma^T C\, \sigma dA - t \int_A u^T F\, dA - \int_{s_u} u^T T\, ds$$

where

σ = stress component matrix

C = elastic compliance matrix

u = prescribed displacements over s_u

u = displacement over s

T = boundary traction over s

A = area of element

F = body forces

s_u = boundary of A over which displacements are prescribed

s = boundary of A

t = thickness (assumed unity)

The variational principle then states that of all the admissable stresses and displacements, the actual solution, that is the one that satisfies compatibility, equilibrium and boundary conditions in A, is distinguished by the stationary value of π_c with respect to variations of σ in A and u_i over s and s_u.

The extremum of the functional is also subject to the constraint conditions

$$\nabla\sigma + F = 0$$

$$\sigma\nu = T$$

where

ν = unit normal vector to s

Simply stated, the admissible stresses must be continuous in A and satisfy the equilibrium equations, and be compatible with prescribed boundary tractions. Admissible displacements must satisfy the prescribed boundary displacements over s_u.

In the hybrid model, the stress in the element and the displacement along the boundary are assumed separately. A typical element is shown in Figure 6. For such an element, the stresses are given as

$$\sigma = P\,\beta$$

where

β = unknown stress parameters satisfying the equilibrium equations.

The only requirement on the number of βs is that there must be a sufficient number to avoid unstable kinematic modes. Let

n = number of nodal degrees of freedom

l = number of rigid body modes

m = number of βs

A necessary condition for a stable solution is that $m \geq n-l$, which, for the case of the rectangular element with four nodes with two degrees of each, means there must be five or more βs. This is, however, only a necessary condition and no sufficient condition is known to exist. The research reported herein uses a five β system the accuracy of which is indicated by Pian [21].

Then

$$P = \begin{Bmatrix} 1 & 0 & 0 & y & 0 \\ 0 & 1 & 0 & 0 & x \\ 0 & 0 & 1 & 0 & 0 \end{Bmatrix}$$

The boundary tractions can be expressed as:

$$T = R\beta = \begin{bmatrix} T_{x_{12}} \\ T_{y_{12}} \\ \cdot \\ \cdot \\ \cdot \\ T_{x_{41}} \\ T_{y_{41}} \end{bmatrix}$$

but for a rectangular element T reduces to

$$T = \begin{bmatrix} 0 & 0 & -1 & 0 & 0 \\ 0 & -1 & 0 & 0 & -x \\ 1 & 0 & 0 & y & 0 \\ 0 & 0 & 1 & 0 & 0 \\ 0 & 0 & 1 & 0 & 0 \\ 0 & 1 & 0 & 0 & x \\ -1 & 0 & 0 & -y & 0 \\ 0 & 0 & -1 & 0 & 0 \end{bmatrix} \beta$$

In this hybrid model, the interelement boundary displacement function u_i is interpolated in terms of the nodal displacements q. That is

$$u = L\, q$$

where

$$L = \begin{bmatrix} (1-x/a) & 0 & x/a & 0 & 0 & 0 & 0 & 0 \\ 0 & (1-x/a) & 0 & x/a & 0 & 0 & 0 & 0 \\ 0 & 0 & (1-y/b) & 0 & y/b & 0 & 0 & 0 \\ 0 & 0 & 0 & (1-y/b) & 0 & y/b & 0 & 0 \\ 0 & 0 & 0 & 0 & x/a & 0 & (1-x/a) & 0 \\ 0 & 0 & 0 & 0 & 0 & x/a & 0 & (1-x/a) \\ (1-y/b) & 0 & 0 & 0 & 0 & 0 & y/b & 0 \\ 0 & (1-y/b) & 0 & 0 & 0 & 0 & 0 & y/b \end{bmatrix}$$

Defining the following matrices

$$H = \int_A P^T C P \, dA$$

$$G = \int_{\partial_A} R^T L \, ds$$

H is determined by a nine point Gaussian quadrature over the area. G is determined by five point quadrature along each applicable boundary segment. The variational functional π_c can then be written

$$\pi_c = 1/2\, \beta^T H \beta - \beta^T G q$$

The stationary condition of the functional with respect to β and q gives

$$H\beta - Gq = 0$$

Solving for β in terms of q gives

$$\beta = H^{-1}Gq$$

If the following is observed

$$k = G^T H^{-1} G$$

Then the variational functional can be written in a form identical to that of the isoparametric elements in the previous section, i.e.,

$$\pi_c = 1/2\, q^T k q - q^T Q$$

The individual element stiffness matrices can then be assembled systematically node by node into a global stiffness matrix. This forms a set of matrix equations, which, when combined with the boundary conditions of the problem, yield the solution to the problem. Both the isoparametric elements and the assumed stress hybrid model use linear interpolation of model displacements, so that the resulting solution to the set of assembled matrix equations will have compatible displacements over the whole domain.

ection IV: Hybrid Stress Finite Element Analysis in Fracture Mechanics of Adhesive Joints

The study of fracture of adhesive bonded joints has become of great commercial interest as the use of such joints becomes more widespread. The study of cracks in adhesive joints appears broken into two general areas. First, there are the primarily experimental studies, such as those of Mostovoy and Ripling [24] or Jermian and Ventrice [25]. Second, there is the study of fracture by use of the FEM by both conventional displacement models, such as Wilson [26], Trantina [26,27], Anderson, *et al.* [28], and Williams [29], as well as hybrid stress models which include a singularity in the assumed stress field [23,30-32].

Although the experimental determination of the strain energy release rate in a cracked monolithic material is widely used, there is some question as to its applicability, particularly to the lap shear configuration. For the symmetric case, such as the double edge notch specimen, the results for G_I [24] compare very closely with those calculated by an exact conformal mapping technique by Bowie [33]. G_I and k_I are related for a monolithic material through the expression:

$$G_I = \frac{\pi (\kappa + 1) k_I}{8 G}$$

where

G = shear modulus

κ = $3-4\nu$ for plane strain and $(3-\nu)/(1+\nu)$ for plane stress

ν = Poisson's ratio

Current, yet to be published work by McGarry, Wang and Mandell at M.I.T. shows that the above expression also applies to adhesive joints if the shear modulus and Poisson ratio of the adhesive are used. This is true because the characteristic length of the singularity at the crack tip is much, much less than the characteristic length of the joint which was found to be the adhesive thickness. The basis of this experimental approach is to determine dC/da, or the change in compliance with respect to crack length. In the double cantilever beam case, simple beam theory gives a very good approximation of the compliance as the crack length changes, so it is not unexpected that the results are reasonable [24]. In the lap shear configuration, the determination of the compliance is a non-trivial problem, due to the complex geometry, its unknown relationship with rotation, and differential straining of the joint. The strain energy release rate approach was used by Jermian and Ventrice [25], but how they arrived at their expression for dC/da is not clear from their reported research.

The normal displacement model FEM has a great deal of difficulty handling the crack tip region in a fracture problem, even in the cracked monolithic material. Even with an extremely fine mesh in the vicinity of the crack tip, such as that used by Trantina [27], the estimate of $\mathcal{G}_I$ is only 25% of that computed by Bowie for the symmetric problem. Anderson, *et al.* [28] and Williams [29] have applied relatively large constant strain elements to the interfacial fracture problem. Due to the type of element (constant strain), and the relative coarseness of the mesh (.002 inch) for the type of problem, it is not surprising that their solution shows sharp oscillations about the analytic solution [34].

The first work in the FEM to incorporate stress singularities in the assumed stress hybrid model contained only a term in $1/\sqrt{r}$ [23,30]. The later work includes higher order singular

terms to more accurately account for the stress singularity at the tip of the crack [31,32]. It is this latter approach which is used as the basis for the super element used at the crack tip in the research reported herein.

The formulation of the super element uses the complex variable stress function formulation of Muskhelishvili [37]. The H and G matrix are then formed by line integrations in the complex plane along each segment, shown in Figure 7. Although the symmetic five node element has been used and gives good agreement with the exact solution, the complete nine node super element has never been perfected prior to the research reported herein. During the course of this study, it was found that the last two rows of the stiffness matrix published by Lasry [31] are in error and some of the formulations in the paper by Tony [32] are also incorrect. The correct stiffness matrix for the nine node super element is included as Table 3. The stiffness matrix given by Lasry yields non-symmetric displacements for the problem shown in Figure 8. It should be noted here that the Aeroelastics Laboratory at MIT has corrected their solution of the stiffness matrix.

The stress intensity factors are shown [32] to be:

$$k_I = \sqrt{2}\beta_1$$

$$k_{II} = \sqrt{2}\beta_{N+1}$$

The research reported herein uses N = 9, which meets the previously stated necessary condition to avoid unstable kinematic modes. The assumed stress hybrid super element is also a stiffness method, and the resulting element stiffness matrix can be assembled as with the element stiffness matrices of the other elements to form the matrix equations. The super

element also uses a linear interpolation function between each two nodes which ensures inter-element compatibility of the displacement solution with the other elements discussed above.

Section V: Results of Analysis of Joint Without Crack

The single most important factor to examine when solving a problem by a numerical technique is the stability of the solution with respect to changes in the characteristic parameters of the method. That is to say, although convergence proofs do exist for the FEM [35], it can only be said that the finite element solution approaches the exact solution as the mesh size becomes "small." The first task in a numerical solution scheme is to determine what "small" is for the specific problem at hand. In a problem for which an exact analytic solution exists, this determination can be made by selecting the mesh arrangement that is acceptably close to the analytic solution. In the adhesive bonded lap shear problem, no such exact solution exists. The fact that no exact solution does exist requires that a stable solution be found.

Determination of a stable mesh size must be done systematically for two reasons. First, the computation time required to solve the problem is proportional to the square of the band width of the matrix equations and linearly proportional to the total number of degrees of freedom. That is

$$t = c\,(n^2 + \text{d.o.f.})$$

where

n = band width of matrix equations

d.o.f. = total degrees of freedom

Therefore, the decrease of mesh dimensions has a highly non-linear effect on computation time. Second, a mesh that is too small may give an inaccurate solution to the problem due to round off error in computation. Roundoff error is greatly reduced in the research reported herein by doing all computation in a double precision mode.

Figure 9 shows a plot of the peel stress, σ_y, at the end of lap along the interface between adherend and adhesive for various meshes. The stability was checked in locations other than along the interface and for stresses other than the peel stress, but the results with respect to solution stability were the same. The latter is not surprising when one considers that it is the displacement field which is converging on the correct solution. Because all stresses are a function of nodal displacement only, all stresses should converge in a similar manner.

Figure 10 shows the mesh arrangement for the critical region in the vicinity of the end of lap. Of primary interest is the use of eight elements across the adhesive layer. The large number of elements across the adhesive thickness provides for the definition of the variation of stress across the thickness. This has not been reported previously, either analytically or numerically, although it has been stated qualitatively by Hahn [15] from his experimental research. Figure 12 shows the variation in normal or peel stress across the adhesive thickness at various distances along the lap. Figure 13 is a similar plot for shear stress.

The strain across the interface physically must be continuous, since both materials (adherend and adhesive) are continuously connected. Because the strain is continuous, longitudinal stress will be different in the two materials due to different elastic properties. To satisfy compatibility, however, peel stress and shear stress (τ_{xy}) must be continuous. It is significant to note that although it is possible to introduce a constraint condition into the

formulation of the problem, the imposition of strict stress continuity in σ_y and τ_{xy} across the adherend adhesive interface was not done. Therefore, in determining the value of σ_y or τ_{xy} at the interface, an extrapolation must be done, both from the adhesive side and the adherend side. If the two values agree, there is a high degree of confidence in the actual value along the interface. Such extrapolations from both sides of the interface were done for all values presented on the interface, and it was found that the two extrapolations agreed within plotting accuracy. Thus, there is a strong case for the reliability of stress values along the interface.

Figure 12 and 13 present the variation in stress across the adhesive thickness for only one modulus ratio of the nine ratios used. It was found that the same trend appears throughout: the gradient in stress is greater near the end of the lap. The lap is highly non-linear in stress near the upper adherend and becomes roughly linear within about one adhesive thickness and nearly constant across the thickness in about five adhesive thicknesses. The non-linear behavior near the end of the lap is much more pronounced for low modulus ratios.

As discussed in Section II, the analytical and numerical literature on adhesive bonded lap joints does not address longitudinal stress in the adherend. This is a serious shortcoming in light of the experimental evidence [4,15] of failures occuring in the adherend due to local bending at the end of the lap. Figure 14 shows the longitudinal stress in the adherend at the interface; since the strain is continuous, the longitudinal stress in the adhesive is much lower. As shown in Figure 14, however, the stress concentration may be sufficiently high to cause yielding, or failure, if a low strength adherend such as 1100 aluminum is used.

The longitudinal stress concentration reduces somewhat as the modulus ratio increases. This reduction is to be expected as differential straining becomes more important relative to

rotation and as the adhesive becomes more flexible. The reduction in longitudinal stress with change in moduli ratio is small, however, varying only from 4.8 for a modulus ratio of one to about 4.1 for a modulus ratio of one thousand.

For a fixed modulus ratio, the longitudinal stress concentration increases with increasing adhesive thickness. This is due to the increased rotation caused by increased eccentricity of the applied loading. The magnitude of the longitudinal stress concentration varies from 4.2 for an adhesive thickness of 2.5 mils to 4.9 for an adhesive thickness of 20 mils (fixed modulus ratio of 20).

Figures 15 through 20 give additional data on the variation in stress from one interface to the other. Previous solutions to the problem have indicated that the stresses are symmetric about the center of the lap. Figures 15 and 16 show the error in that assumption. In both the moduli ratios of commercial importance in adhesive joints (20 and 200), shown in Figures 15 and 16, the fillet shape at the end of the lap has greatly relaxed the stress in the vicinity of point A (Figure 15) compared to the stress in the vicinity of point B (Figure 16). Modulus ratio 2 shows a behavior more nearly like a homogeneous material, i.e., it is very strongly influenced by geometric discontinuities. That is, modulus ratio two shows an inflexion indicating a relaxation of stresses similar to modulus ratios 20 and 200, but upon continuing toward the geometric discontinuity, the singular behavior at the discontinuity overwhelms the relaxation trend.

Figure 17 and Figure 18 are the same data as Figures 15 and 16, but "normalized" by the value of σ_y at point B'. Point B' is the value of stress at the centroid of the closest element to point B, extrapolated to the interface by the method discussed above. The distance from point

B, which is the actual end of lap, to point B$'$ is 0.1 adhesive thicknesses. Although the general shape of the curves is not affected, Figures 17 and 18 do make it easier to see the distance to which the perturbation is observed in the joint. Much higher absolute values of peel stress are found for low moduli ratios, as shown in Figures 15 and 16, but Figures 17 and 18 show how rapidly these decay. Perturbation distance is of the order of only one adhesive thickness for modulus ratio 2, and increases for the more flexible modulus ratios to about 5 thicknesses for ratio 200.

Figures 19 and 20 are the shear stresses along the interface normalized by the value at point B$'$. Here, again, the fillet shape at point A has virtually eliminated the stress concentration in the higher moduli ratios. The perturbation distance for shear is greater than that for peel, as would be expected from the eccentric loading of the single lap joint.

Figures 21 and 22 give the peeling stress and shear stress at the midplane of the bond. As seen in Figures 2 and 3, the midplane solution is very close to the Goland and Reissner solution in the critical end of the lap region. As the earlier figures have shown, the maximum stress occurs at the adherend-adhesive interface, and the midplane is a conservative location of stress concentration. The numerical technique of Wooley and Carver [10] loses the peak stress of point B$'$ due to the use of only two constant strain elements across the thickness. If the values for stress obtained in the research herein are arithmetically averaged through the thickness, they are very close to the other numerical solutions (which internally average due to the nature of the constant strain elements), such as those of Wooley and Carver, which lends weight to the reliability of the solution reported herein.

Figure 23 is included to show the variation in the maximum peel stress and maximum

shear stress at point B' as the modulus ratio changes over three orders of magnitude. The maximum stress decreases monotonically as modulus ratio increases. This is because the more flexible adhesive layers can distribute the effect of geometric discontinuities over a greater distance as shown by larger perturbation distances for the higher moduli ratios.

Figure 24 shows the variation in peel stress along the interface in the vicinity of point B for various adhesive thicknesses. From the Figure, it is seen that the maximum change in slope for all thicknesses occurs at roughly the same location, which supports the earlier finding, i.e., that perturbation distance is primarily a function of the moduli ratio. The results of Figure 24 must be interpreted carefully for the following reasons. First, the analysis scheme used does not take into consideration thermal elastic effects or residual stress, both of which become more important for thicker adhesive layers. That means that the fact that the loading condition does not produce a large stress concentration in the joint may be unimportant, if the joint is at the point of incipient failure due to shrinkage-induced residual stresses. Second, failure is statistical in nature, and the larger the joint, the more likely a failure producing flaw is to exist [19]. Third, a joint with a thicker adhesive layer will have less dimensional stability due to the lower modulus and, therefore, larger strains in the adhesive. Finally, as shown earlier, the longitudinal stress in the adherend is increased for greater adhesive thicknesses, and may induce plastic deformation, or even failure, in the adherend. The seriousness of these thickness effects can be appreciated when one considers that the range of adhesive thicknesses normally used fall within the range of three to ten mils.

Section VI: Results of Analysis of Joint with Short Edge Crack

As discussed in Section V, the first step in the numerical solution of a problem for which no analytic solution exists is to determine stability of the solution. The determination of a stable solution when using an assumed stress hybrid super element is more complicated due to the nature of the element. Unlike the conventional displacement model of the FEM, where smaller elements yield a closer approximation to the exact solution (not countng round off error), the super element, being a numerically exact solution including singular and higher order terms [33], yields a better solution for a larger element. Because the crack tip super element is surrounded by normal elements, however, the overall quality of the stress field determination is a trade off between a super element that is as large as possible, and surrounding elements that are as small as practical.

The super element must be sufficiently large to contain the singular behavior. Because the stress gradient is still very large at the interelement boundary between the super element and the surrounding elements, a study of the mesh size in the vicinity of the crack tip is necessary to determine a stable solution. The research reported herein did not systematically determine the optimum mesh arrangement. As seen in Figure 25, however, the $1/\sqrt{r}$ singular behavior of stress does end within the superelement. In addition, a vast amount of work has been done on the fracture problem of adhesive joints by Dr. Wang, M.I.T. Materials Science and Engineering Department, using the five node symmetric super element. In the course of his work, optimum mesh arrangements were determined for a similar adhesive joint system, and, therefore, the mesh arrangement shown in Figure 11, which was used in the work reported here, was not a purely arbitrary choice. The mesh chosen conformed to the optimum mesh

arrangement determined by Dr. Wang's work, and, therefore, the solution reported herein is estimated to be within one half percent of the converged solution. Because no solution exists to the problem of an adhesive bonded lap joint with an edge crack, the results reported herein are a significant initial input to the continuing research on this problem.

One interesting result arising from the analysis of the adhesive bonded lap joint with a short edge crack is shown in Figure 26. This figure is a plot of log stress intensity factor k_I (opening mode) and k_{II} (inplane shear mode) vs log modulus ratio, where these ks are related to the conventional nomenclatures used by NASA and ASTM by the following:

$$K_I = \sqrt{\pi}\ k_I$$

$$K_{II} = \sqrt{\pi}\ k_{II}$$

Figure 26 is significant in that at least for moduli ratios between 2 and 200, both the opening mode stress intensity factor and the inplane shear mode stress intensity factor plot as straight lines in log-log. The slopes of these lines are 0.49 for k_I and 0.46 for k_{II}. This implies that

$$k_I = C_1\ (E/E_a)^{0.49}$$

$$k_{II} = C_2\ (E/E_a)^{0.46}$$

where C_1 and C_2 are constants dependent on the nominal load, crack length and other geometric variables of the problem. Such a relation must be systematically investigated further to determine if the power law relating the modulus ratio to the stress intensity factor is itself a function of the geometric variables.

A comparison of the solution to the lap shear problem with and without a short edge crack permits the following observations:

1. Interfacial stresses at the end of the lap without a crack are identical to those found in Section V for the uncracked solution.

2. Longitudinal stress concentrations in the adherend along the interface are the same as the uncracked case except that the location of the maximum longitudinal stress moves toward the center of lap by approximately one half the crack length.

3. Far field stresses in the adherends are identical for both cracked and uncracked solutions.

4. Stresses in the crack flank are relaxed, from those found in the end of lap of the uncracked case. (Figures 15-20 vs. Figures 27-29)

The first three points indicate that the presence of a short crack does not affect the stiffness of the joint as a whole. If the stiffness were significantly affected, there would be an increased longitudinal stress from the additional bending required to accommodate additional rotation, or the far field stresses would begin to change, or both.

By comparing Figures 27 and 28 with Figures 16 and 20, respectively, the drastic effect on the interfacial stresses along the upper interface due to the presence of the crack can be seen. Similarly, a comparison of Figure 29 with Figures 15 and 19 shows the effect along the lower interface. Both top and bottom interfaces show a compressive σ_y in the crack flank region. In the case of the upper adherend, the general state of compression in the adhesive in the crack flank may be due to the relatively stiff adherend pulling the otherwise relaxed material up against the still intact adhesive material. In the lower adherend (Figure 29), the compression may be a secondary effect: due to the larger longitudinal stress in the region than in the uncracked case, the discontinuity in material properties causes a slight compression.

It is significant that the displacement solution shows the crack is actually open. This is sensible since the uncracked solution shows a tensile stress or peeling stress. It is also

significant to note that the stress intensity factors are of the same order of magnitude, with k_{II} actually being somewhat larger than k_I (see Table 4). This indicates the failure is mixed mode, rather than opening mode only, as cited in some experimental work [25]. Again this is sensible, physically.

A further implication from current results may indicate that if the adhesive material is sufficiently ductile to accommodate the singularity at the crack tip by local plastic deformation rather than by brittle fracture, then the interfacial peel stress and the shear stress values could be lower than the end of lap stresses for the uncracked problem. This indicates that the perturbation distance of the stress intensity at the crack tip is no greater than the perturbation distance of the stress concentration due to the geometric discontinuity of the uncracked problem, which then implies that the perturbation distance is more strongly a function of material properties (as seen in Section V) than of geometry.

Section VII: Summary and Conclusions

The first part of the research examined the solution of the single lap shear adhesive joint with no crack. The improvement of the results with respect to earlier efforts is due to two factors. First, assumed stress hybrid elements were used in most of the critical areas of the problem. Since the hybrid element yields the same degree of accuracy as a second order displacement model [21], it is inherently more accurate than the constant strain elements used in previous numerical solutions [10,11] or "classical" solutions which do not address stress in the adhesive at all. Second is the use of more elements across the adhesive layer to determine the variation in stress across the layer and to obtain a good approximation of the value of the stress at the interface.

Three conclusions can be drawn from the first part of the research. First, there is a strong stress gradient across the thickness of the adhesive as well as along the lap, particularly in the vicinity of the end of the lap. Second, no solution to the lap shear problem can ignore the longitudinal stress in the adherend as is commonly done in the literature where only the peeling stress and the shear stress are discussed. The importance of the longitudinal stress has been shown experimentally, but it has never before been specifically shown numerically or analytically. Third, the magnitude of the stress at the end of the lap is higher than previously reported. This is a result of the assumption of an infinitessimal adhesive thickness in the analytical solutions and due to the use of constant strain elements and a mesh that was too coarse in earlier numerical solutions.

The second part of the research is the examination of the adhesive bonded single lap joint with a short edge crack. An assumed stress hybrid super element was used at the crack tip which includes terms capable of describing the singular behavior at the crack tip. It is significant that this is the first known fully operational computer program utilizing the general nine node super element and, therefore, the first application of the element to a real problem, and the first analytical attempt to address the adhesive fracture problem with real physical dimensions and material properties.

The results from the second part were not thoroughly investigated and are preliminary in nature. They indicate that the stress intensity factors are related to the modulus ratio by a power law. They also show that the stress intensity factor for inplane shear is not only of the same order of magnitude as the stress intensity factor for the opening mode, but actually slightly larger. The comparability in the magnitude of k_I and k_{II} is contrary to the conclusions

drawn in experimental work such as Mostovoy [24] and others which indicates k_I as being an order of magnitude larger than k_{II}. The fact that most polymeric adhesives are more sensitive to fracture in the opening mode makes experimental determination of inplane effects difficult, which would account for experimental underestimation of k_{II}. The analysis shows that stresses are relieved in the crack flank region and a slight compression exists normal to the interface. Finally, the results from the analysis of the lap joint with a short crack indicate that there is no effect on the uncracked solution in the "far" field, and that far can be interpreted as being of the order of 5-10 adhesive thicknesses along the lap away from the crack tip.

Section VIII: Suggestions for Further Work

The results of the research reported warrant further study of the adhesive bonded lap shear joint. The most promising approach to the problem is a parametric study of the effect of the many variables involved, first in the uncracked case and then using that as a basis in the cracked case. Because no rigorous study of the uncracked case exists, a catalogue of results for the uncracked case must be built up, so the cracked case can be compared to it, to see the effect of the crack.

A parametric study on the uncracked adhesive bonded joints should include not only single lap shear joints, but also double lap shear and scarf joints. For these the effect of the following geometric variables should be investigated, in addition to the effect of different adhesive thickness presented herein:

1. Overlap length - particularly with respect to the effect on longitudinal stress
2. Shape of adhesive at end of lap

3. Non-uniformity of adhesive layer
4. Thickness of adherends
5. Shape of adherends in overlap region, such as the recommendations of Cheery and Harrison [36]

Future work must also study the effect of material variables in addition to the moduli ratio studied herein such as:

1. Dissimilar adherend materials
2. Anisotropic materials
3. Viscoelasticity
4. Material incompressibility
5. Plasticity

All variables mentioned, except the last three, may be studied with the present computer program, but modifications of the formulation are required to handle any of the last three. A systematic study should also include joint loadings other than tensile, such as bending or biaxial stress.

When results are in hand for the uncracked lap joint are determined, all of the variables mentioned for the uncracked case should be studied with respect to various crack variables, such as:

1. Crack length
2. Edge cracks
3. Internal cracks

4. Orientation of crack

The current computer program can handle all the above cases with the noted exceptions (viscoelasticity, material incompresibility, and plasticity). The only problem in continuing the research is manpower and computation expense.

Appendix I

Goland and Reissner Solution to Single Lap Shear Adhesive Joint [1]

$$\tau_{xy} = \frac{T}{4L}\left[\frac{\beta L}{2t}(1+3\kappa)\frac{\cosh(\beta x/t)}{\sinh(\beta L/2t)} + 3(1-\kappa)\right]$$

where

τ_{xy} = shear stress at point x

T = load on lap joint, per unit width

L = length of the overlap

t = thickness of each adherend

x = distance from the center of lap

$$\beta = \frac{8G_a t}{E t_a}$$

$$\kappa = \frac{1}{1 + 2\sqrt{2}\tanh\left(\frac{L}{2t}\sqrt{\frac{3\lambda T}{2Et}}\right)}$$

G_a = shear modulus of adhesive

t_a = thickness of adhesive layer

$$\lambda = 1 - \nu^2$$

ν = Poisson's ratio of adherends

$$\sigma_x = \frac{2\kappa\gamma T}{\Delta L}\left\{\left[\frac{\gamma L}{2t} R_2 - 2\sqrt{2}\,\alpha \cosh\frac{\gamma L}{2t}\cos\frac{\gamma L}{2t}\right]\cosh\frac{\gamma x}{t}\cos\frac{\gamma x}{t} + \left[\frac{\gamma L}{2t} R_1 - 2\sqrt{2}\,\alpha \sinh\frac{\gamma L}{2t}\sin\frac{\gamma L}{2t}\right]\sinh\frac{\gamma x}{t}\sin\frac{\gamma x}{t}\right\}$$

σ_x = peel stress at point x

$$\gamma = \left(\frac{6 E_a t}{E t_a}\right)^{0.25}$$

E_a = Young's modulus of adhesive

$$\Delta = \sinh\frac{\gamma L}{t} + \sinh\frac{\gamma L}{t}$$

$$R_1 = \cosh\frac{\gamma L}{2t}\sin\frac{\gamma L}{2t} + \sinh\frac{\gamma L}{2t}\cos\frac{\gamma L}{2t}$$

$$R_2 = \sinh\frac{\gamma L}{2t}\cos\frac{\gamma L}{2t} - \cosh\frac{\gamma L}{2t}\sin\frac{\gamma L}{2t}$$

$$\alpha = \frac{L}{2t}\sqrt{\frac{3\lambda T}{2Et}}$$

FIGURE 1

Geometric Configuration of Problem

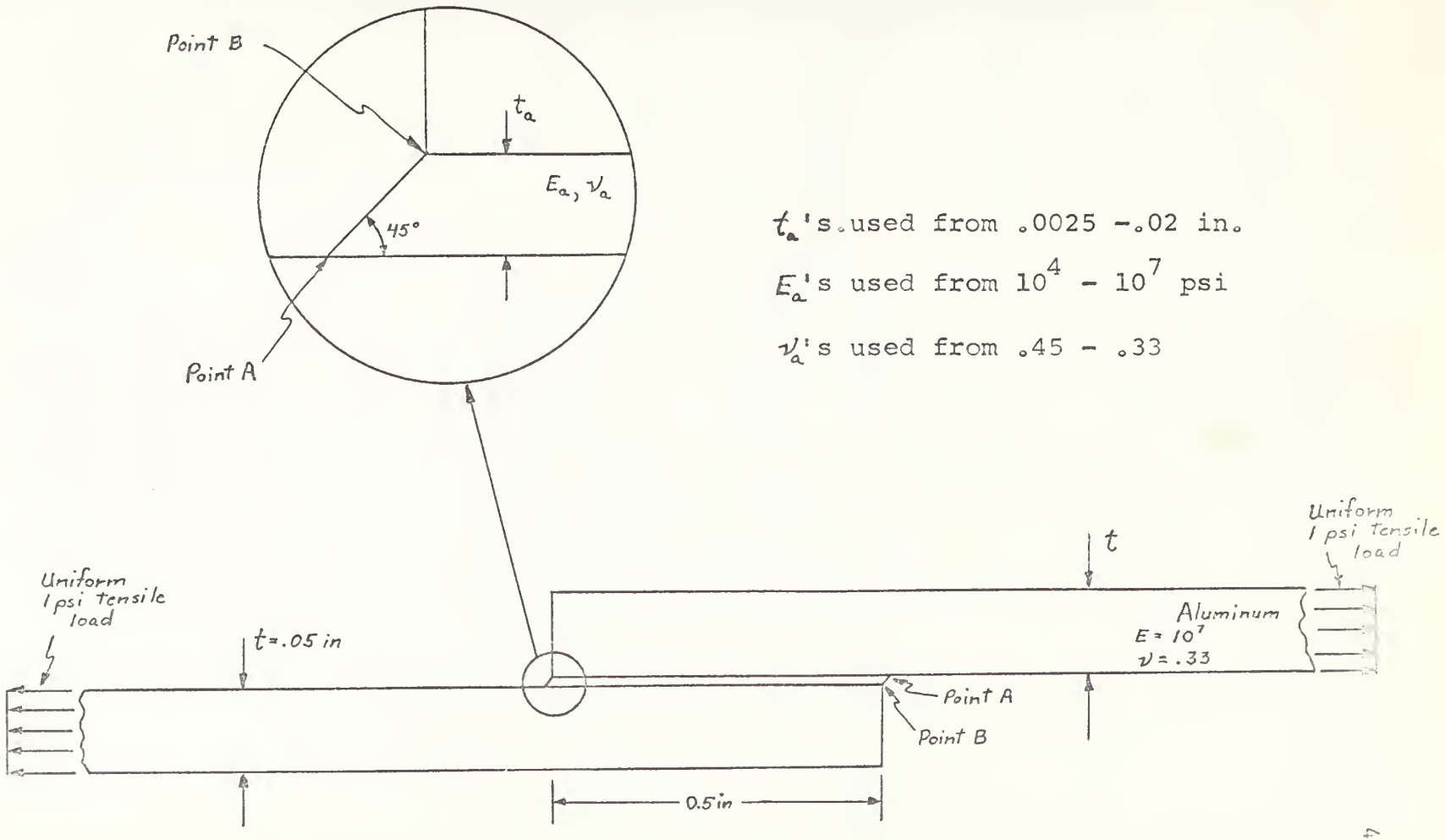

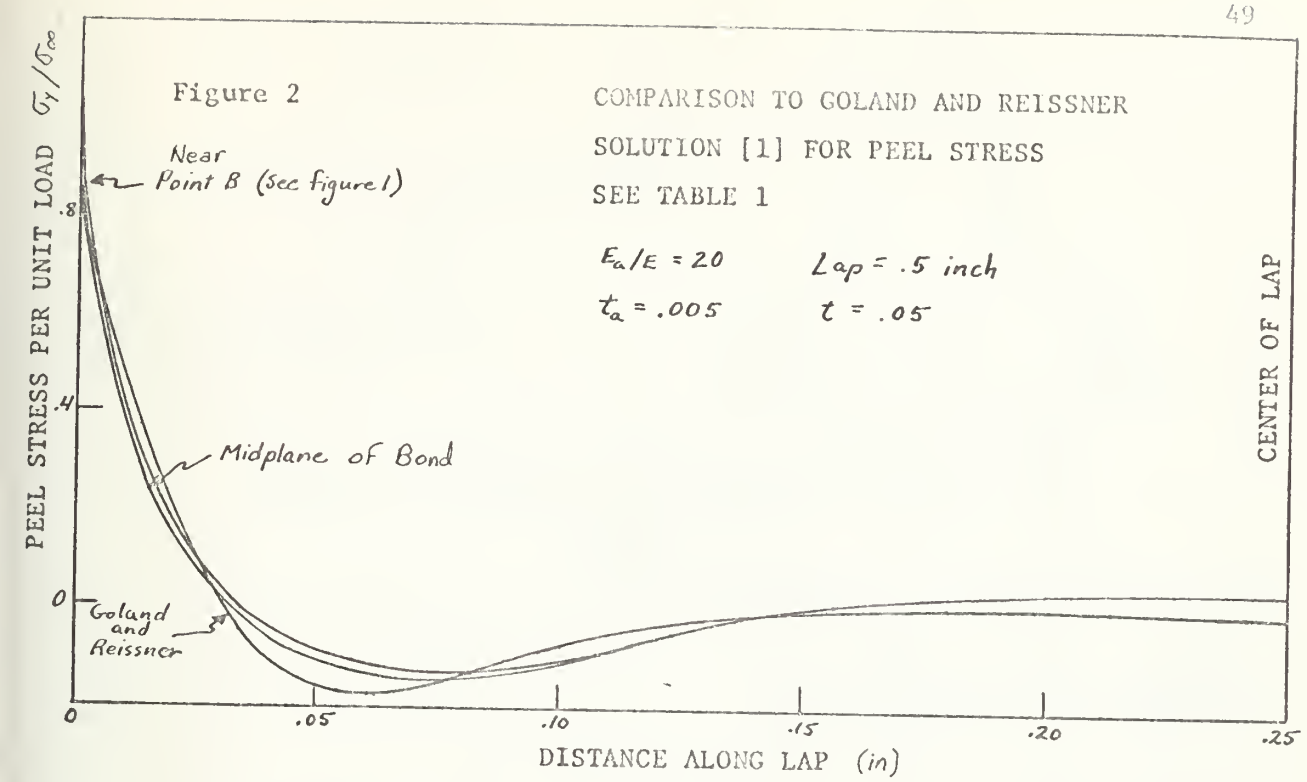

Figure 2

COMPARISON TO GOLAND AND REISSNER SOLUTION [1] FOR PEEL STRESS SEE TABLE 1

$E_a/E = 20$ $\quad Lap = .5$ inch

$t_a = .005$ $\quad t = .05$

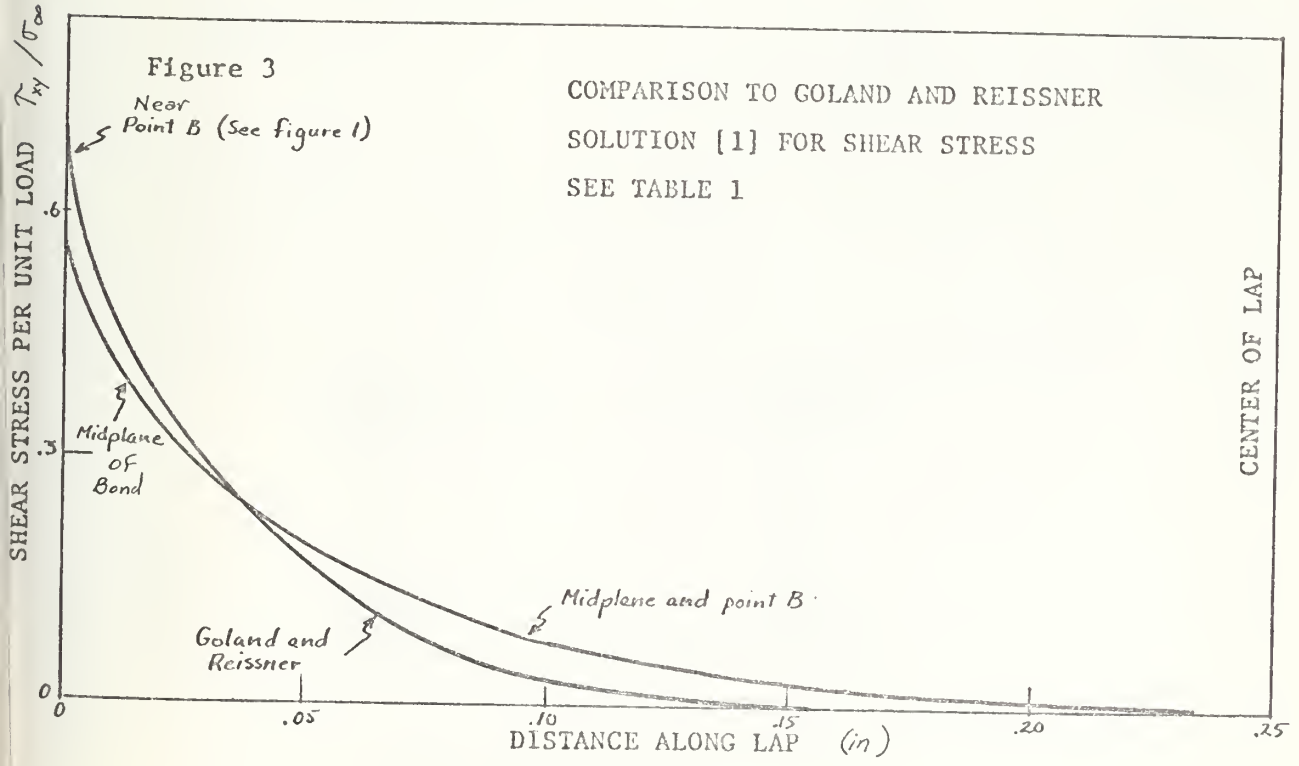

Figure 3

COMPARISON TO GOLAND AND REISSNER SOLUTION [1] FOR SHEAR STRESS SEE TABLE 1

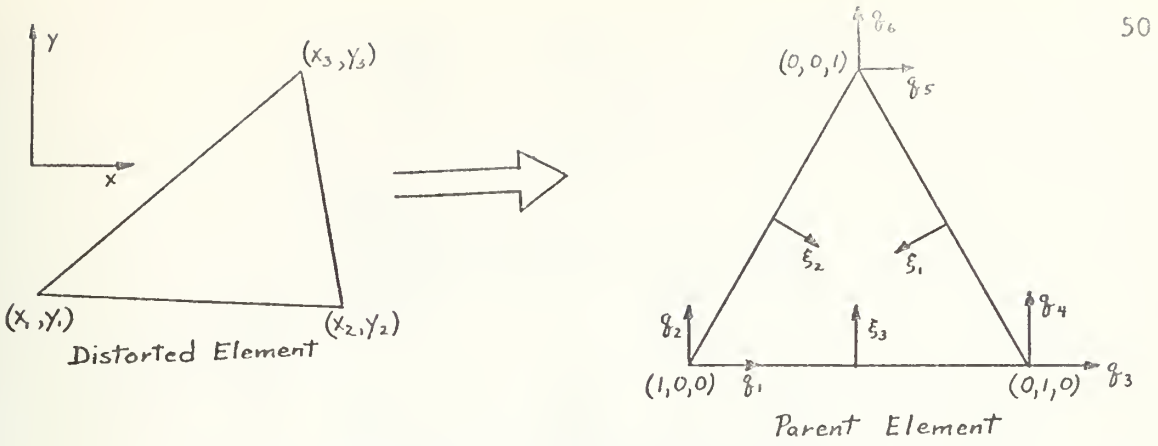

General Triangular Element Transformation

FIGURE 4

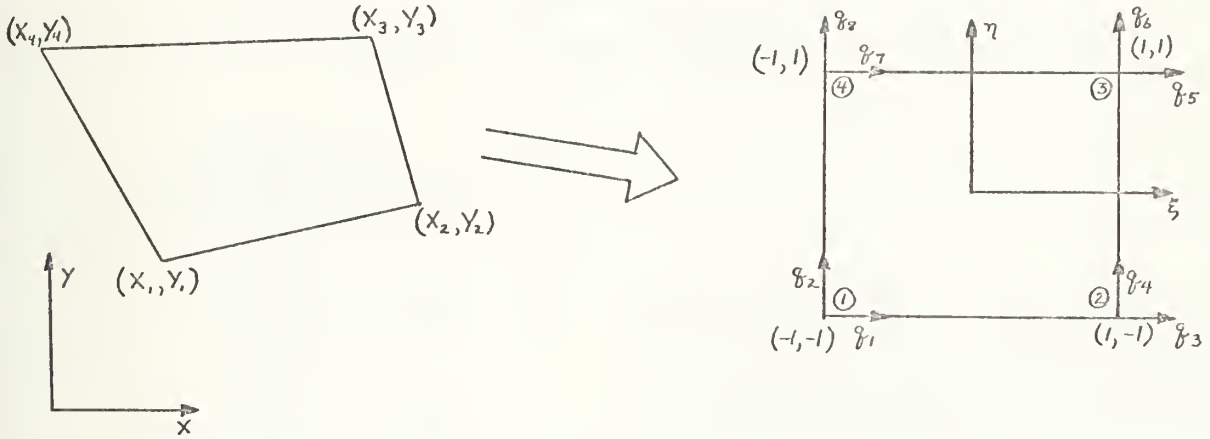

General Quadrilateral Element Transformation

FIGURE 5

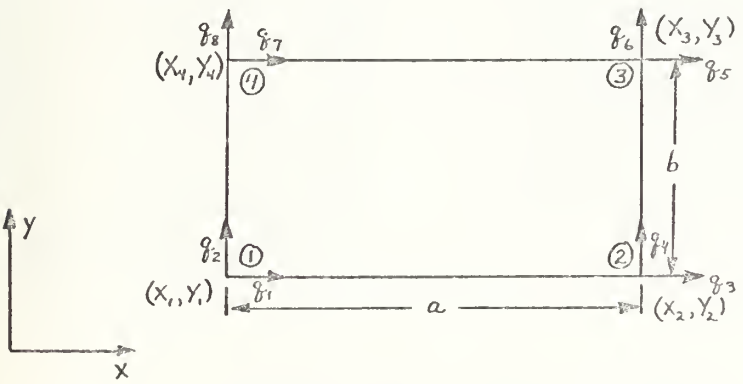

Rectangular Hybrid Element

FIGURE 6

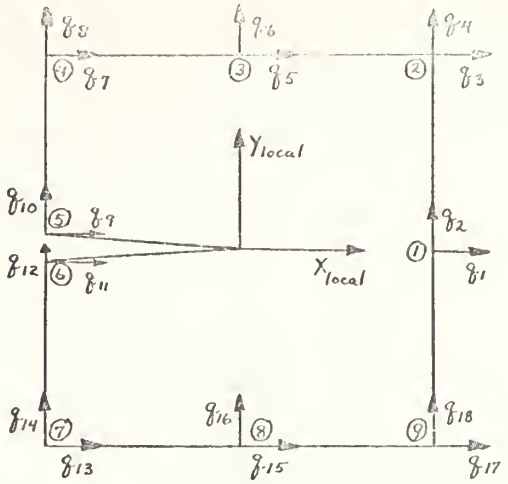

Assumed Stress, HYBRID SUPER ELEMENT

FIGURE 7

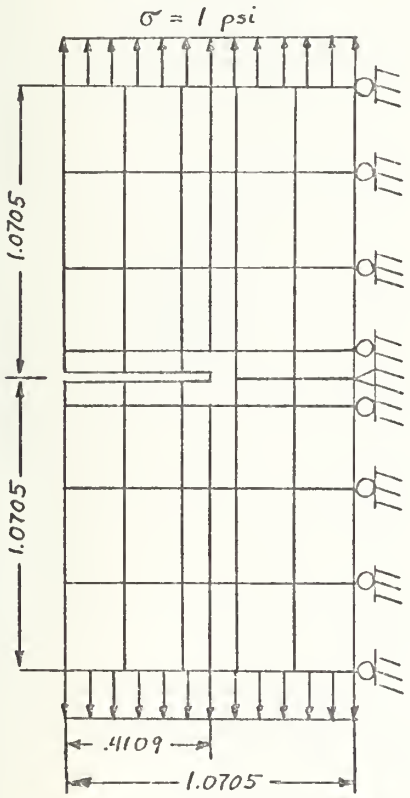

After Bowie [33] , Luk [23]

Edge Crack with Symmetric Loading for Test Element

$E = 1.0$

$\nu = 0.3$

45 Elements
120 Unconstrained degrees of freedom
Lumped loading (at nodes)

(Results in Table 2)

FIGURE 8

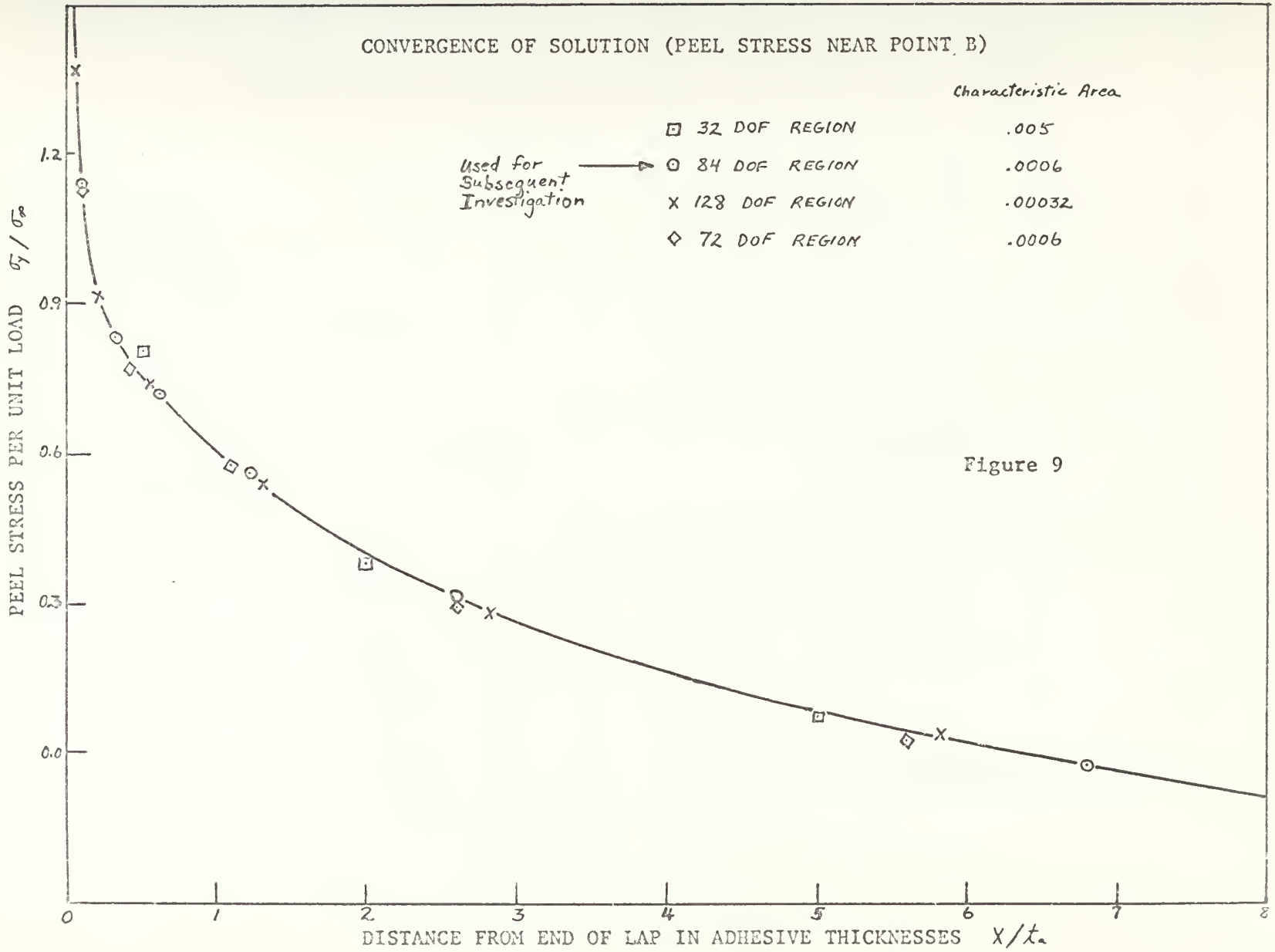
CONVERGENCE OF SOLUTION (PEEL STRESS NEAR POINT B)
Characteristic Area
32 DOF REGION .005
Used for Subsequent Investigation
84 DOF REGION .0006
128 DOF REGION .00032
72 DOF REGION .0006
PEEL STRESS PER UNIT LOAD σ_y / σ_∞
1.2
0.9
0.6
0.3
0.0
0
1
2
3
4
5
6
7
8
DISTANCE FROM END OF LAP IN ADHESIVE THICKNESSES X/t_a

Figure 9

Mesh Arrangement in Vicinity of End of Lap with no Crack

FIGURE 10

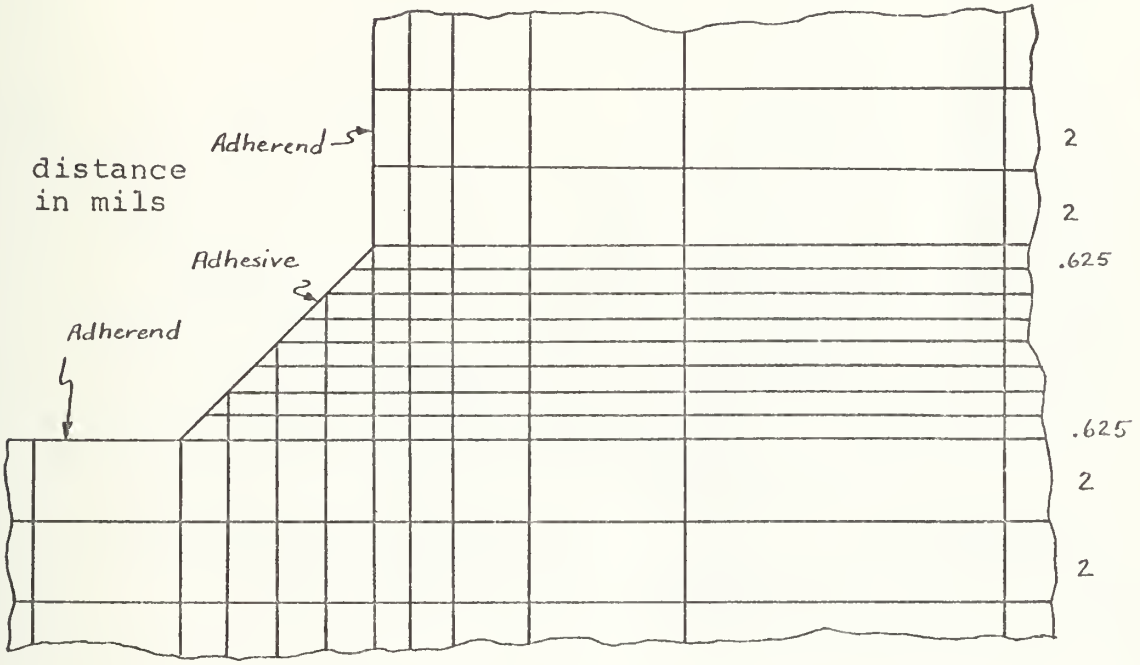

Mesh Arrangement in Vicinity of End of Lap with Short Edge Crack

FIGURE 11

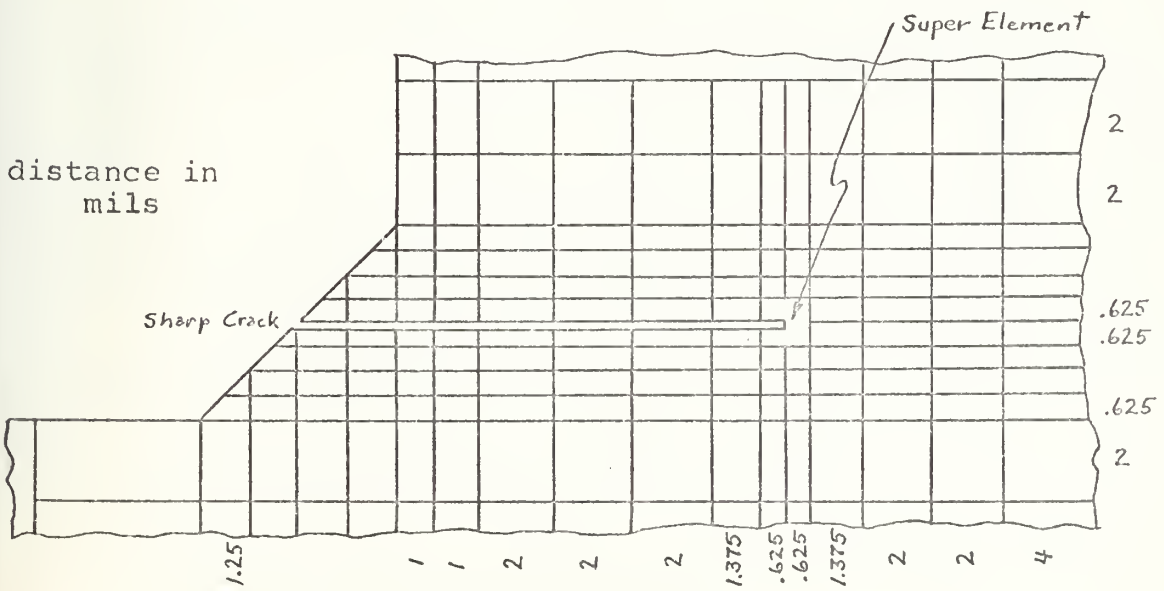

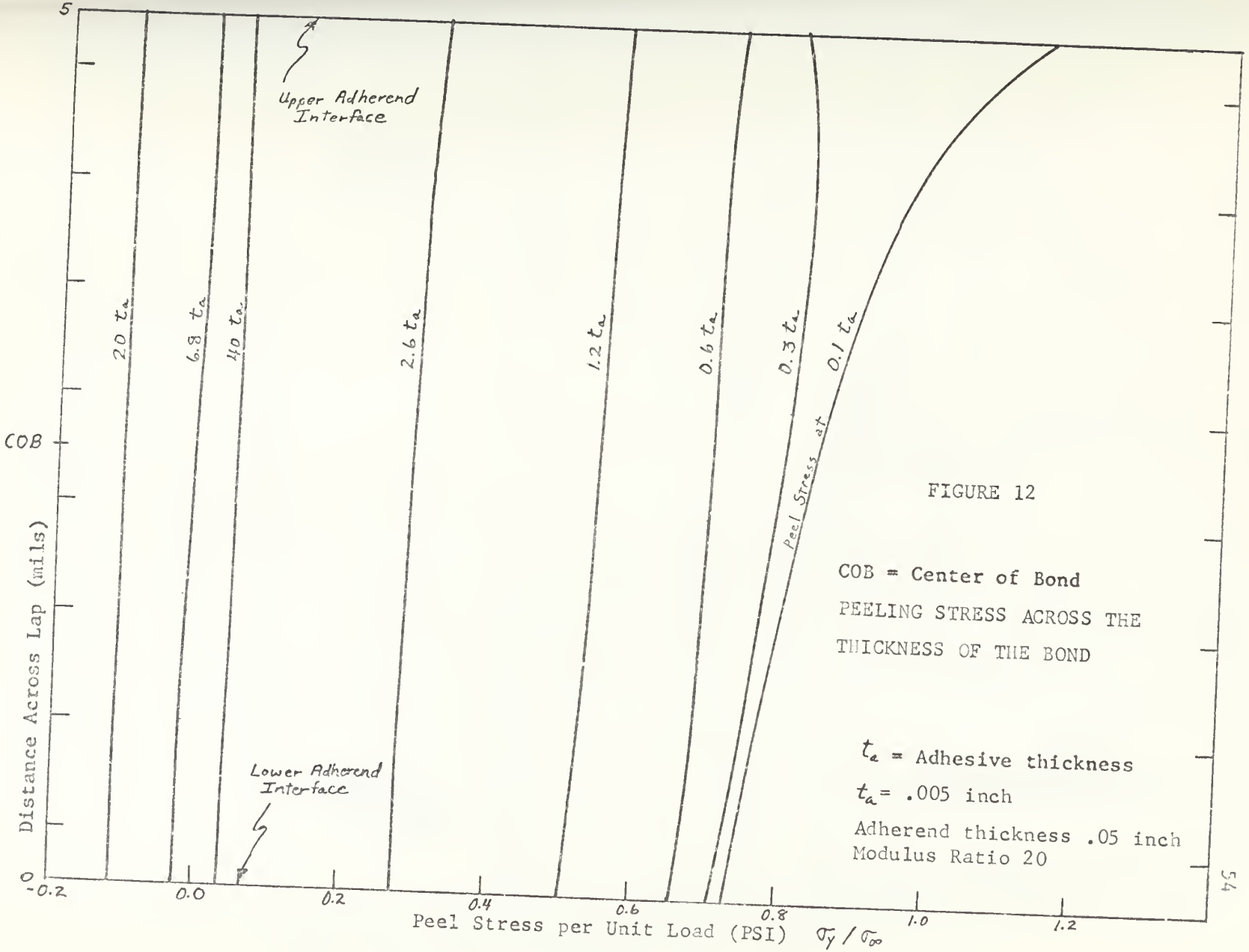

FIGURE 12

COB = Center of Bond

PEELING STRESS ACROSS THE THICKNESS OF THE BOND

t_a = Adhesive thickness

t_a = .005 inch

Adherend thickness .05 inch
Modulus Ratio 20

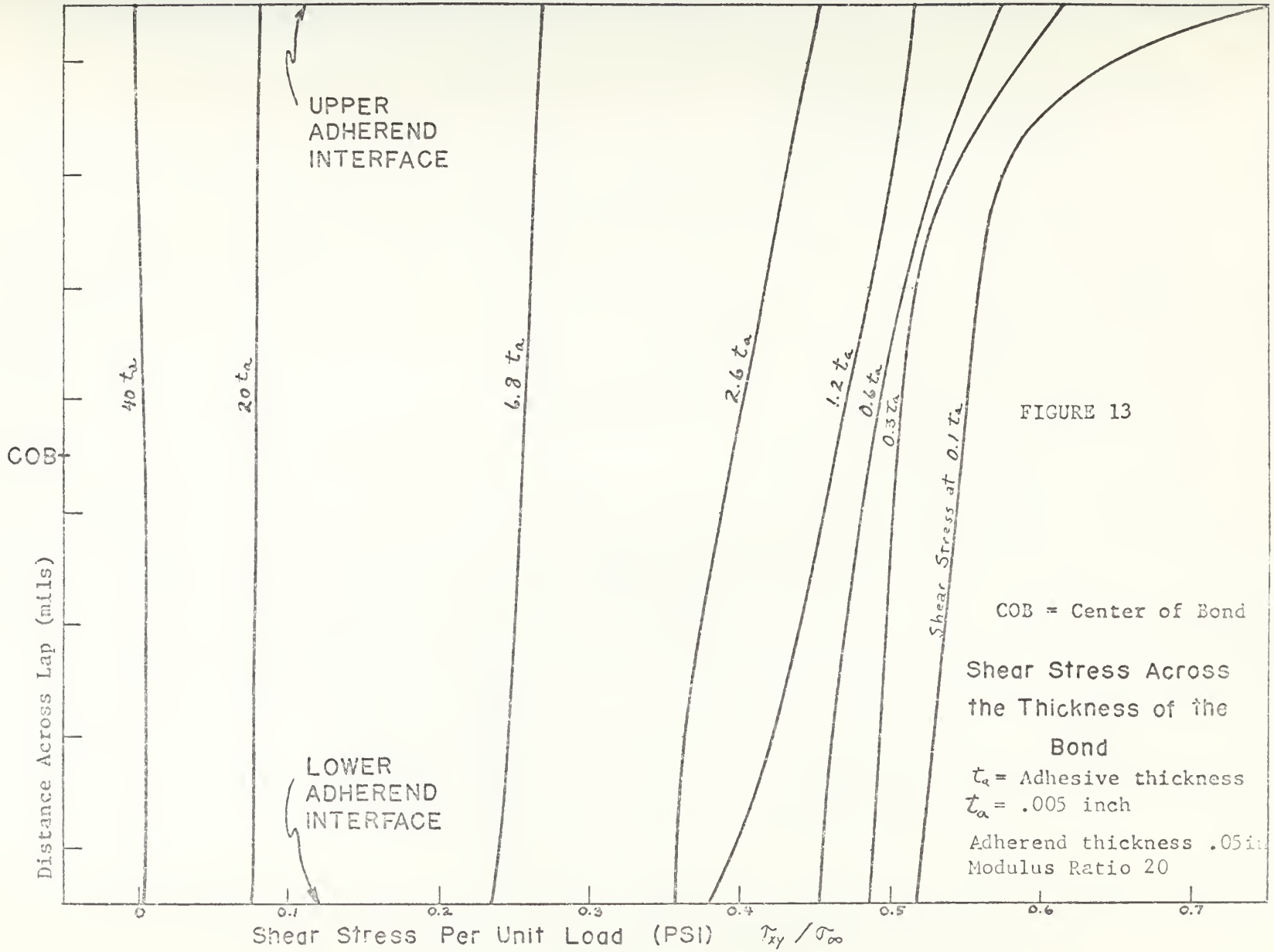

FIGURE 13

COB = Center of Bond

Shear Stress Across the Thickness of the Bond

t_a = Adhesive thickness

t_a = .005 inch

Adherend thickness .05in

Modulus Ratio 20

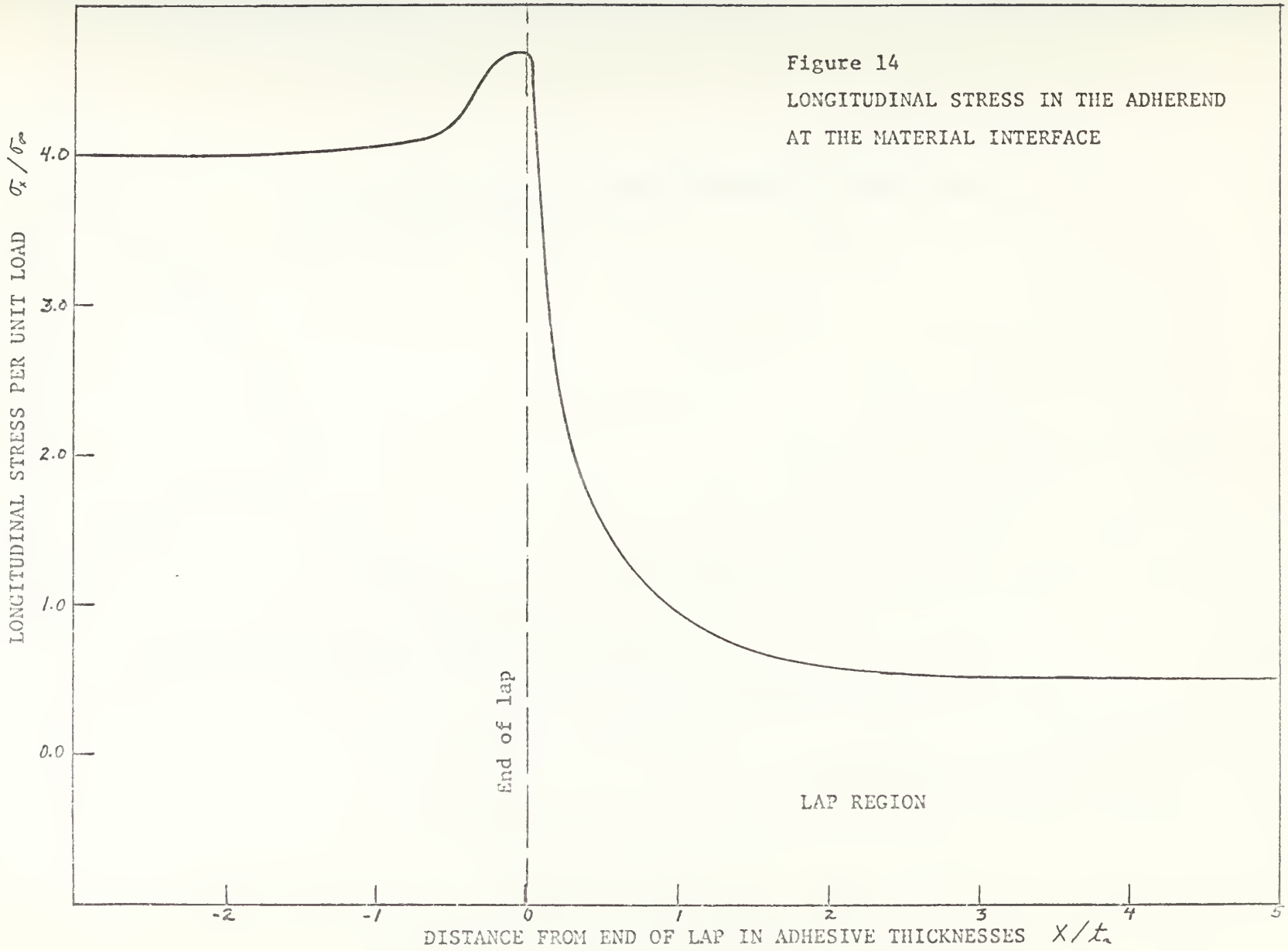

Figure 14

LONGITUDINAL STRESS IN THE ADHEREND AT THE MATERIAL INTERFACE

FIGURE 15

PEELING STRESS ALONG INTERFACE Near Point A (See figure 1)

Selected Moduli Ratios

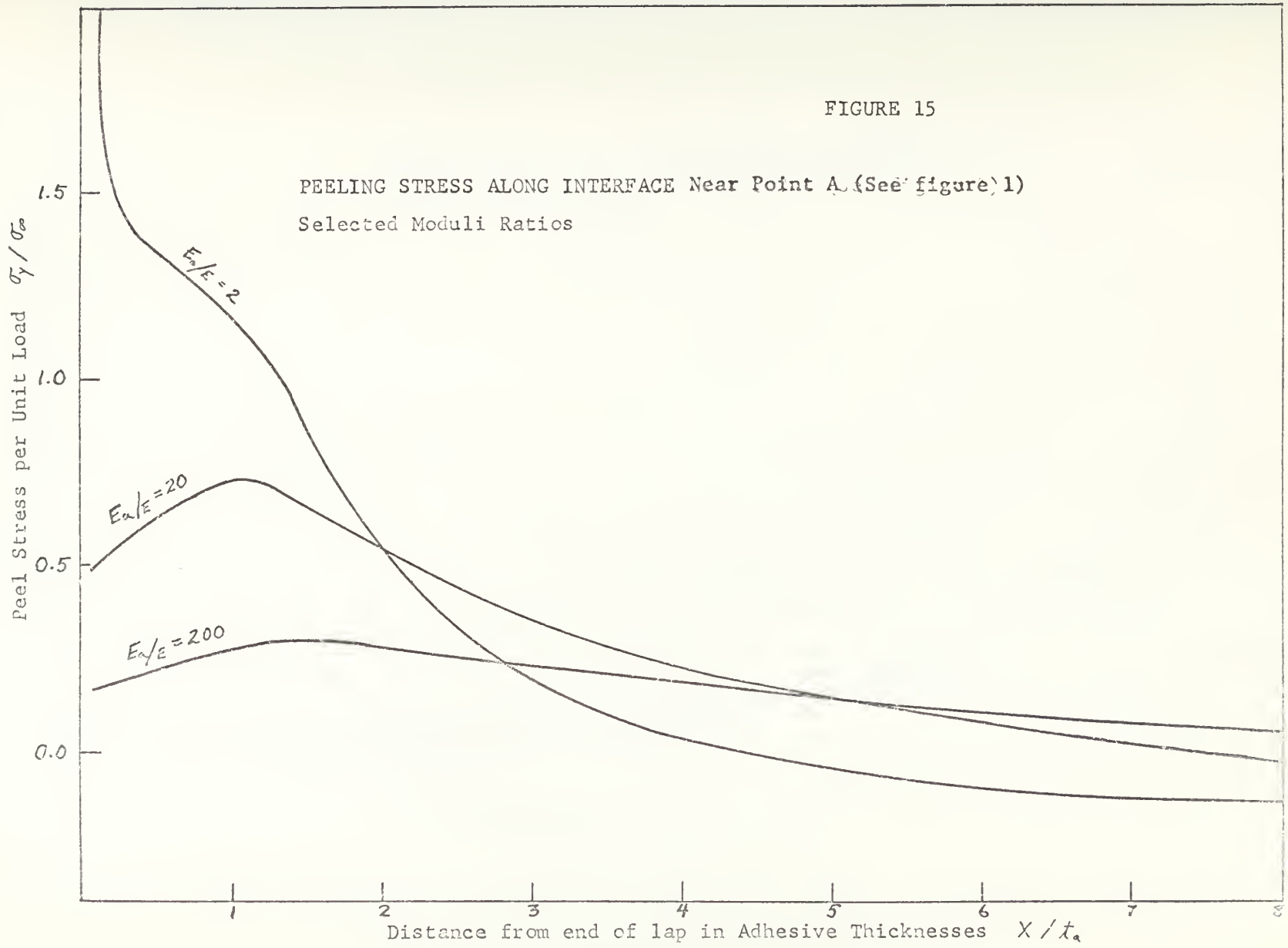

FIGURE 16

PEELING STRESS ALONG INTERFACE NEAR POINT B

Selected Moduli Ratios

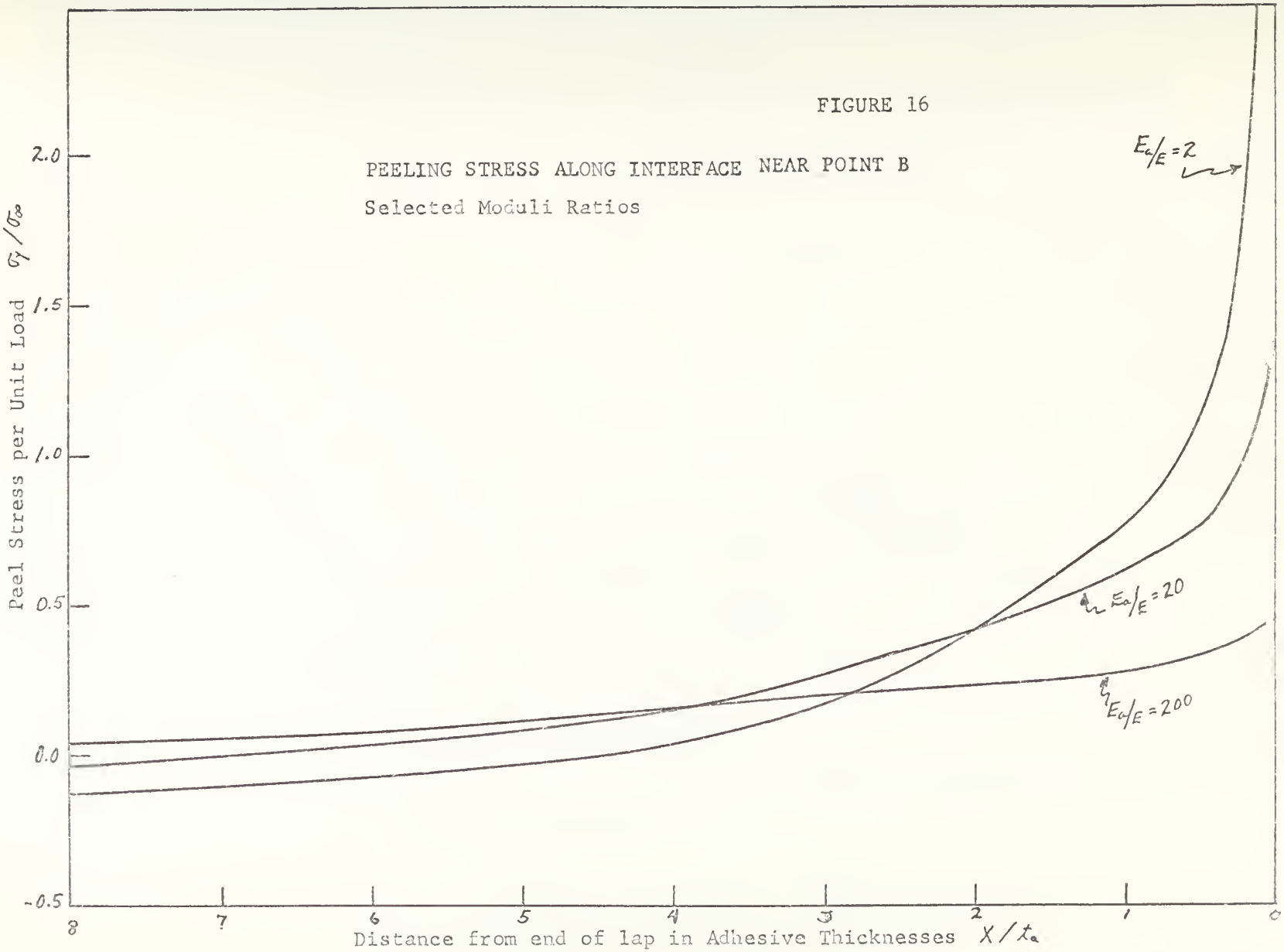

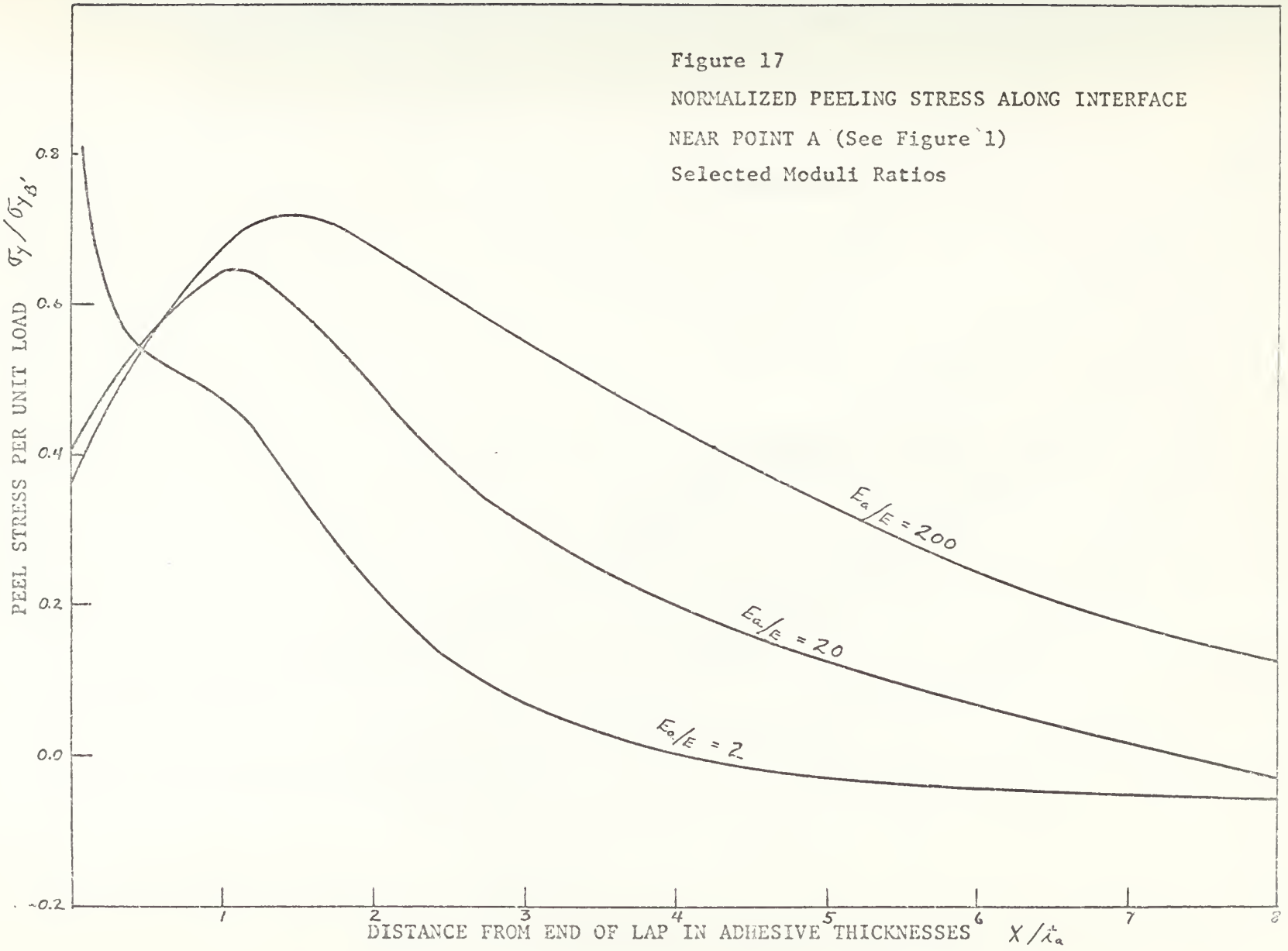

Figure 17

NORMALIZED PEELING STRESS ALONG INTERFACE

NEAR POINT A (See Figure 1)

Selected Moduli Ratios

NORMALIZED PEELING STRESS VS. DISTANCE FROM END OF LAP

Near Point B (See figure 1)

Selected Moduli Ratios

FIGURE 18

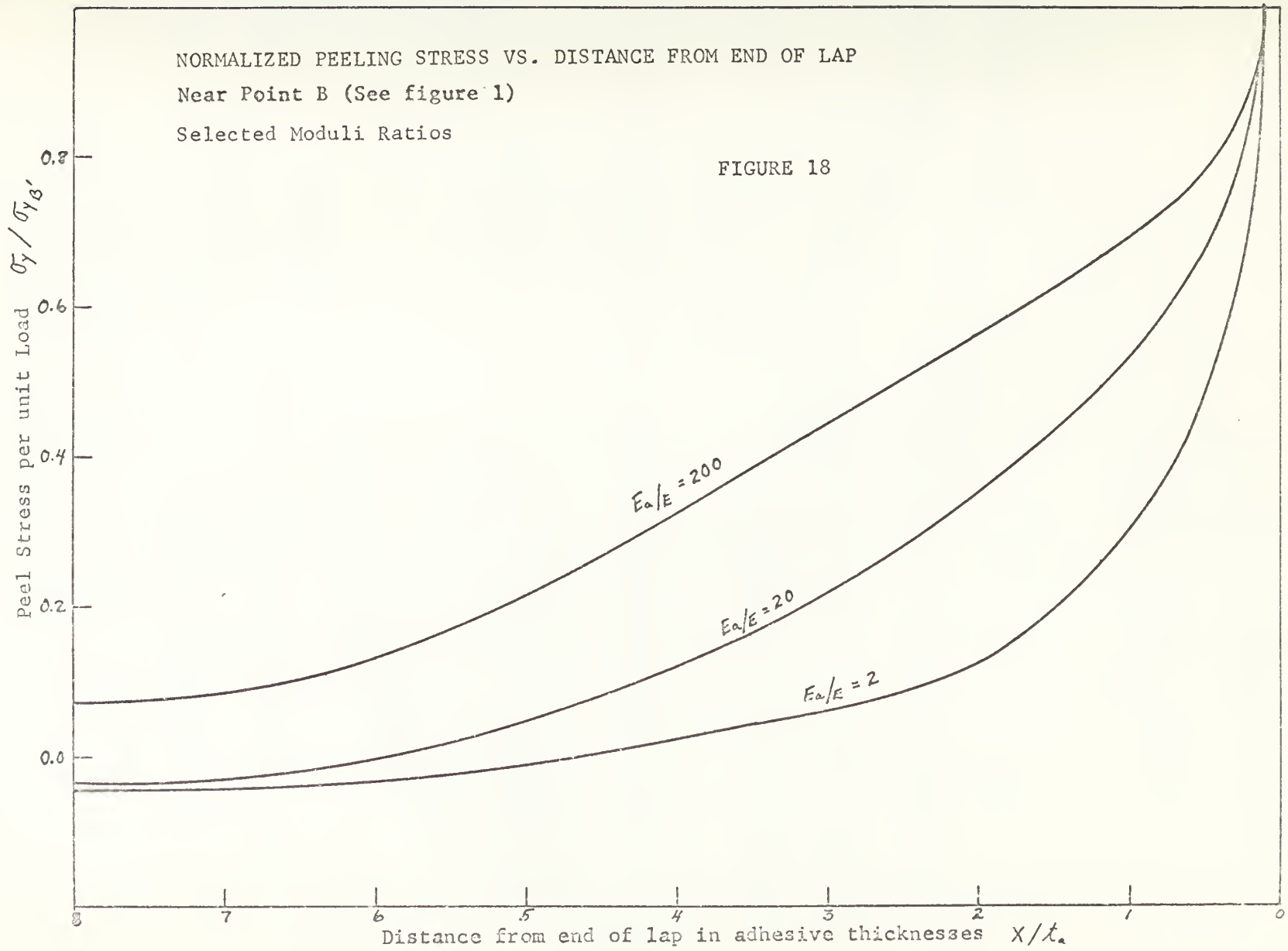

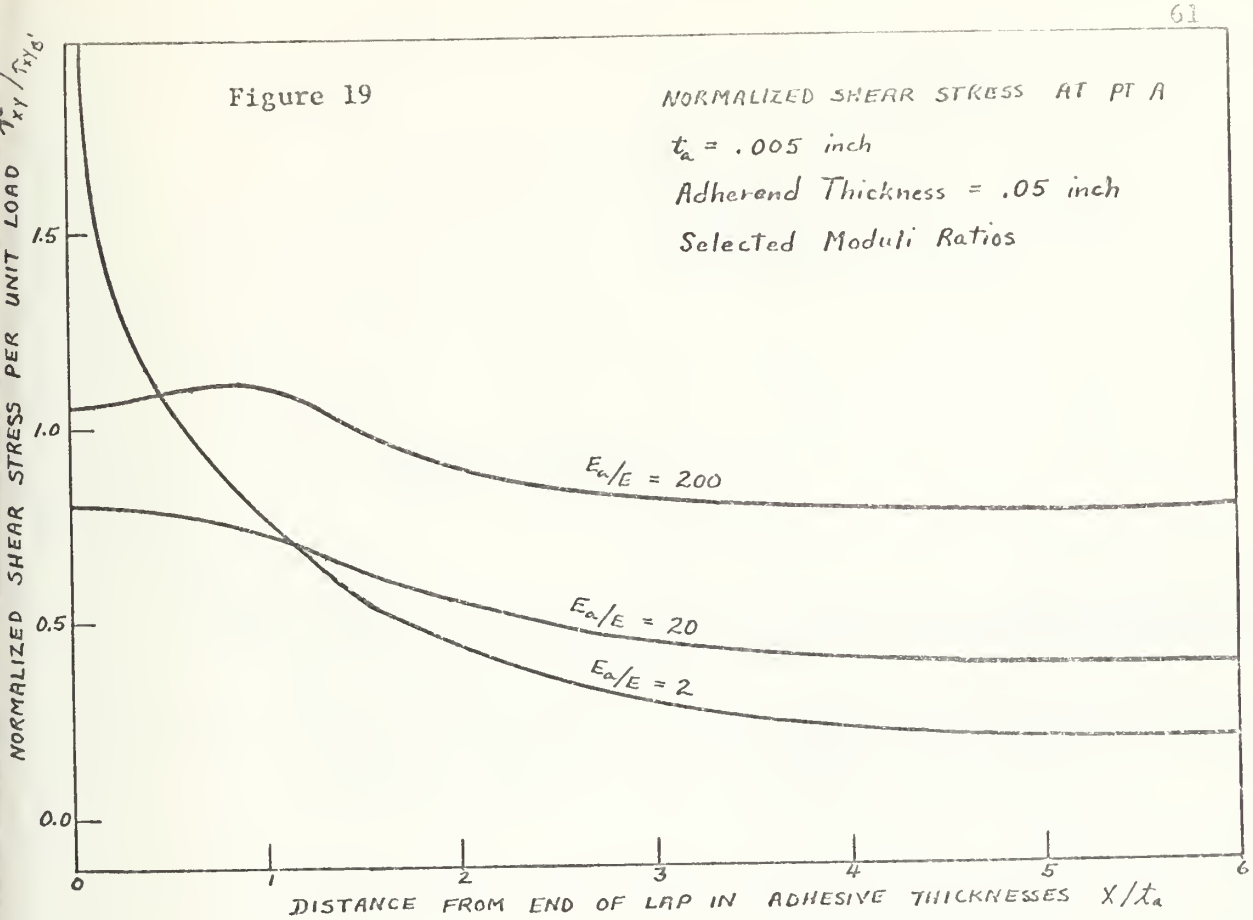

Figure 19

NORMALIZED SHEAR STRESS AT PT A

t_a = .005 inch

Adherend Thickness = .05 inch

Selected Moduli Ratios

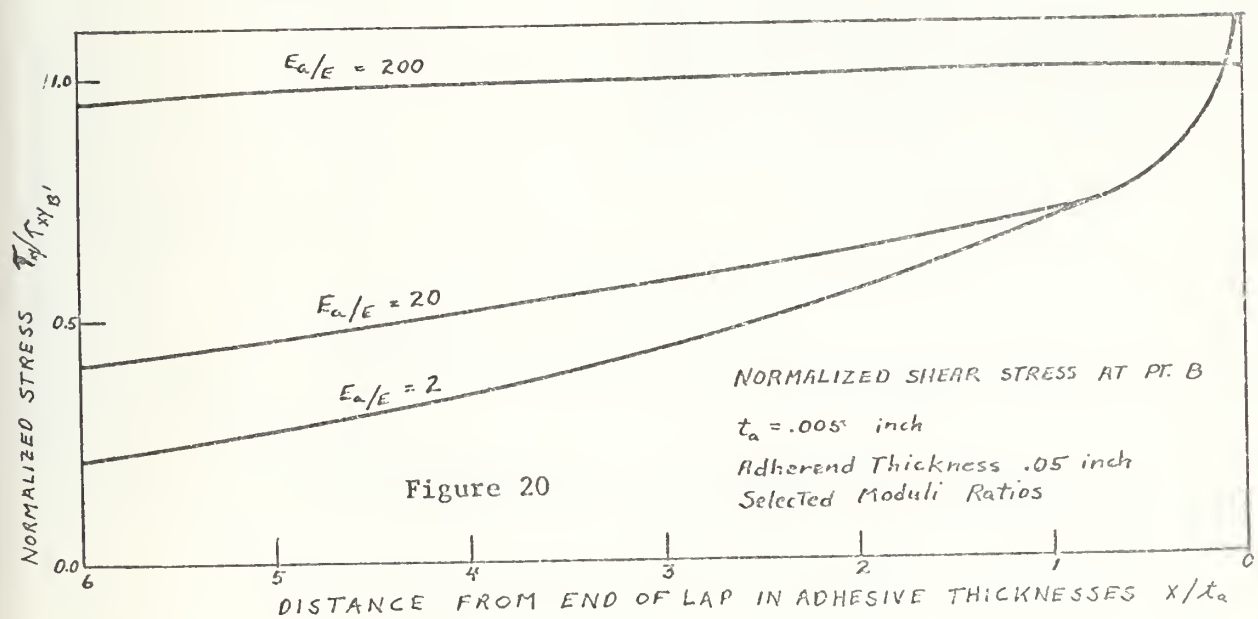

Figure 20

NORMALIZED SHEAR STRESS AT PT. B

t_a = .005 inch

Adherend Thickness .05 inch

Selected Moduli Ratios

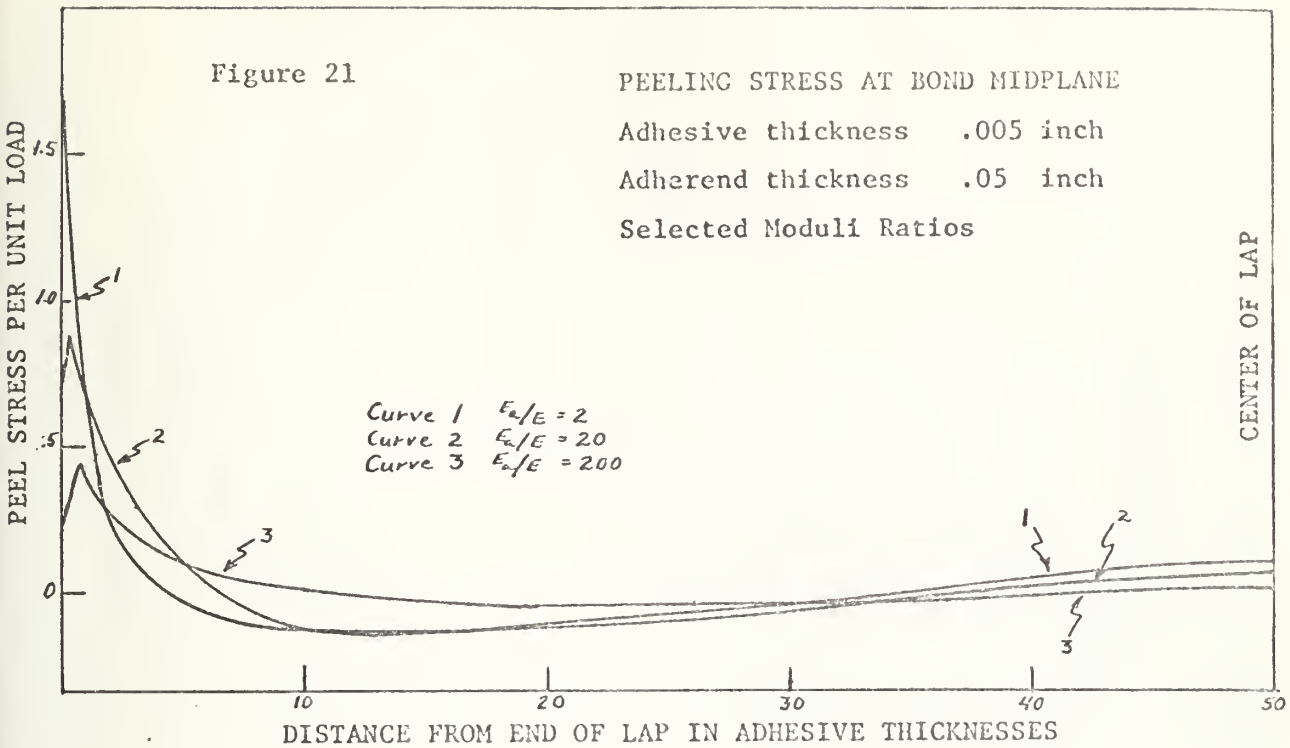

Figure 21

PEELING STRESS AT BOND MIDPLANE
Adhesive thickness .005 inch
Adherend thickness .05 inch
Selected Moduli Ratios

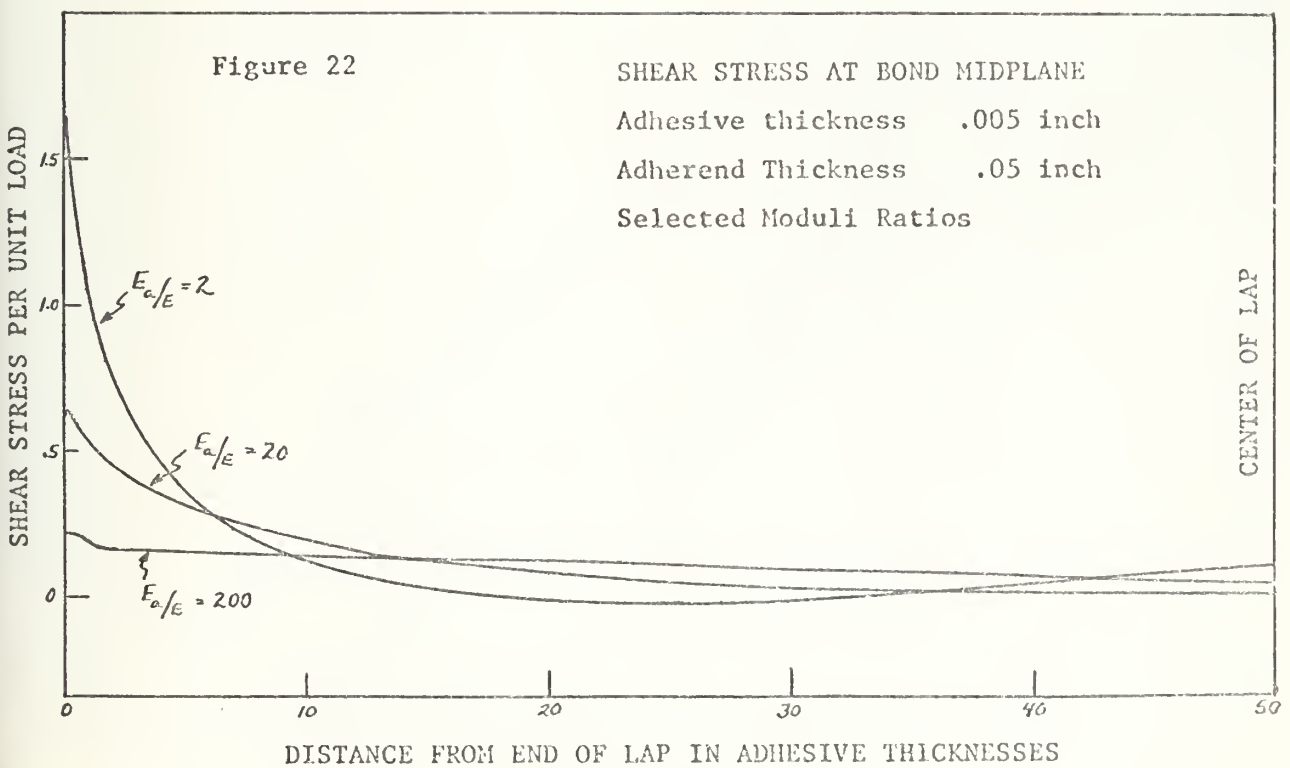

Figure 22

SHEAR STRESS AT BOND MIDPLANE
Adhesive thickness .005 inch
Adherend Thickness .05 inch
Selected Moduli Ratios

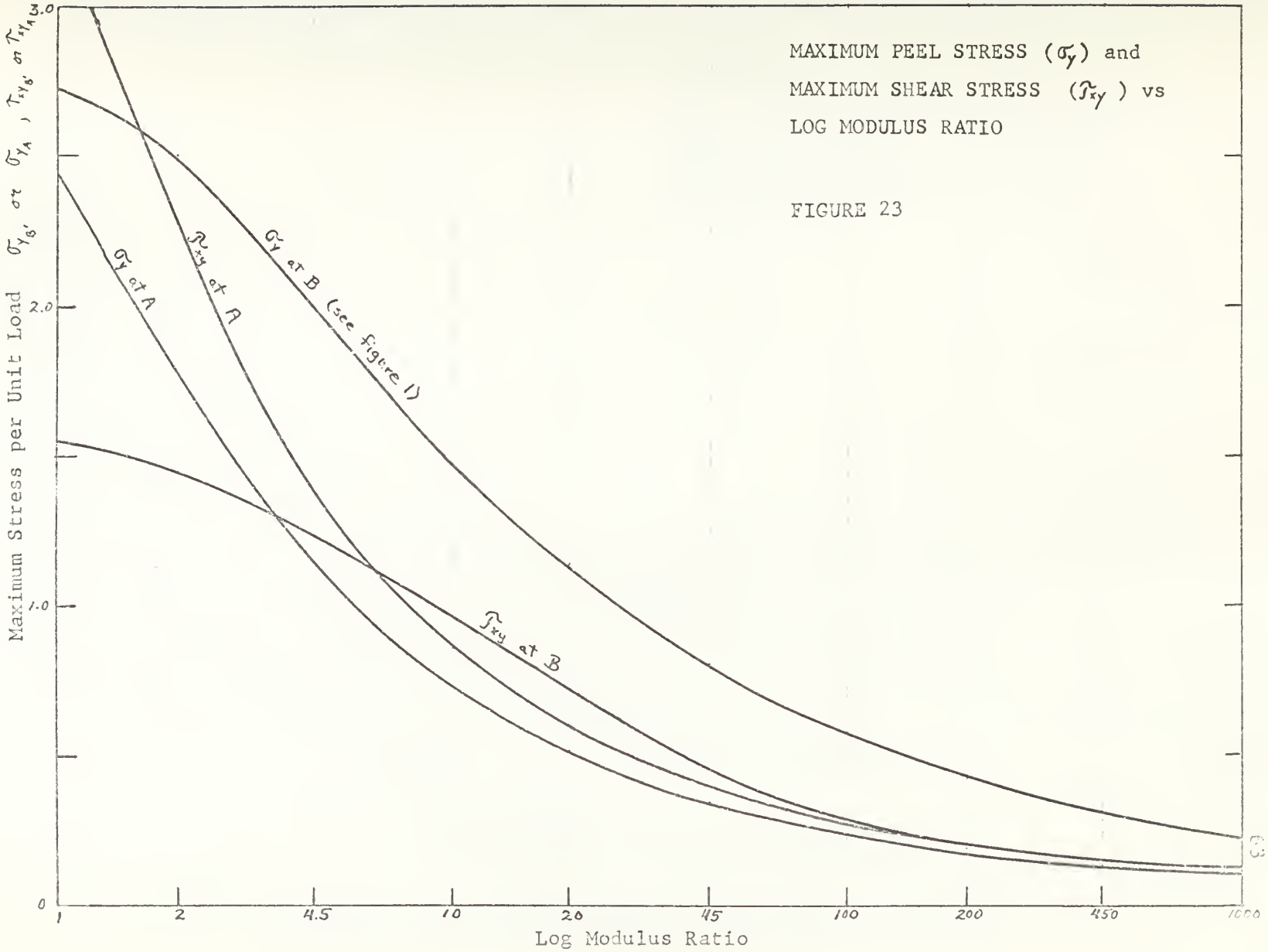
MAXIMUM PEEL STRESS (σ_y) and
MAXIMUM SHEAR STRESS (τ_{xy}) vs
LOG MODULUS RATIO
FIGURE 23
Maximum Stress per Unit Load σ_{y_B}, or σ_{y_A}, τ_{xy_B}, or τ_{xy_A}
3.0
2.0
1.0
0
σ_y at A
τ_{xy} at A
σ_y at B (see figure 1)
τ_{xy} at B
1
2
4.5
10
20
45
100
200
450
1000
Log Modulus Ratio

FIGURE 24

PEEL STRESS NEAR POINT B (See Figure 1)
Selected Adhesive Thicknesses
Modulus Ratio 20
Adherend Thickness .05 inch

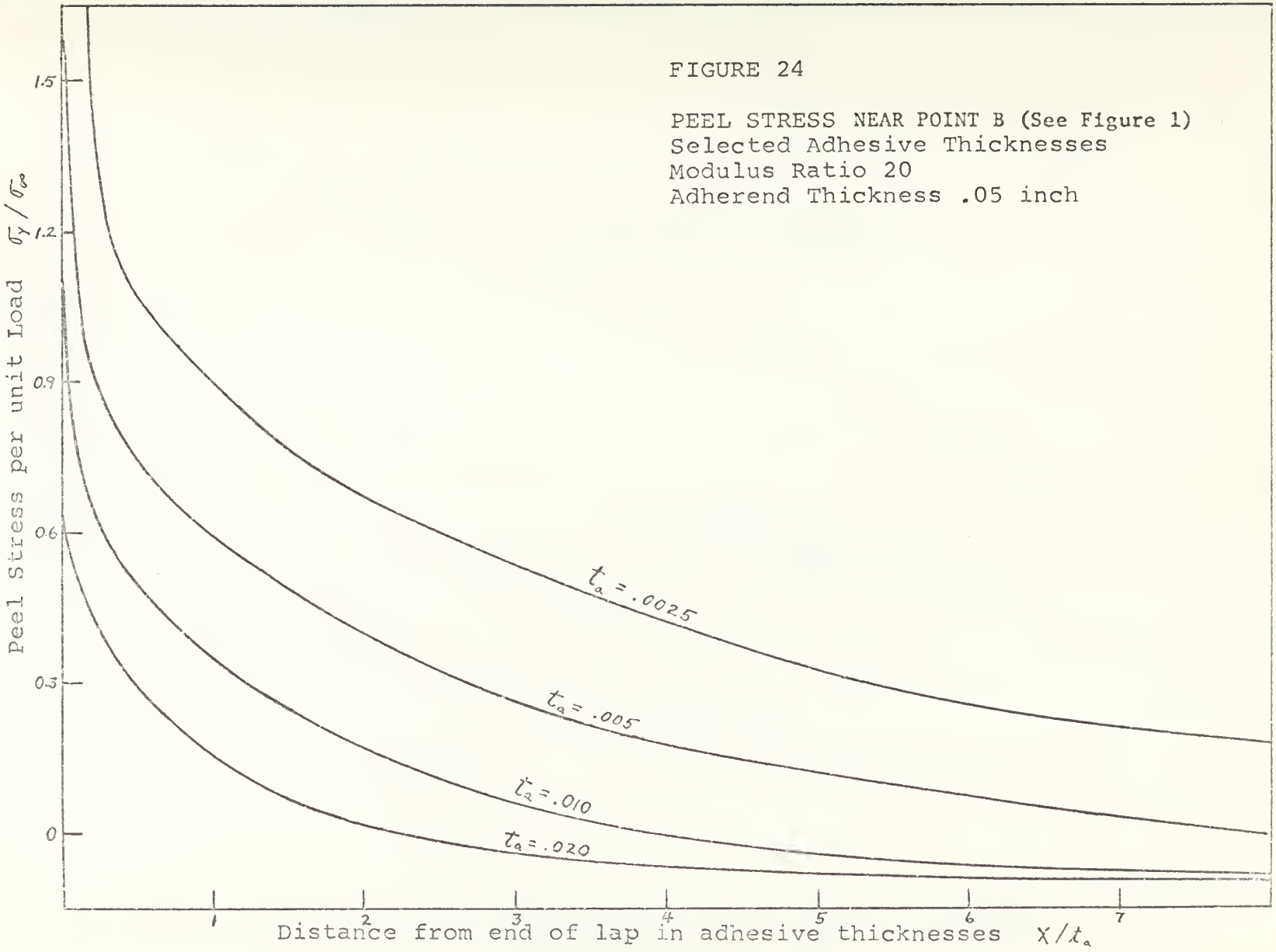

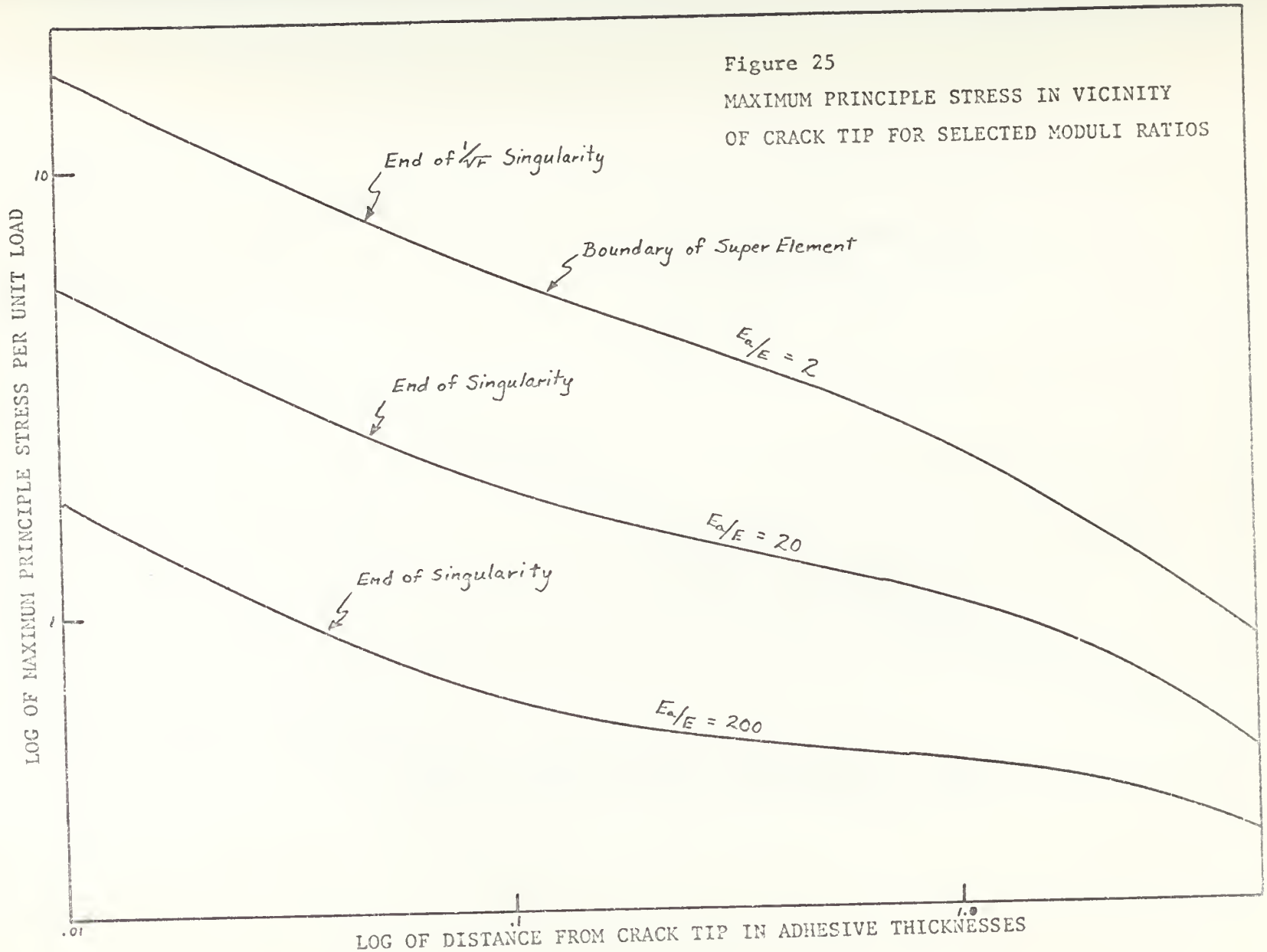
Figure 25
MAXIMUM PRINCIPLE STRESS IN VICINITY
OF CRACK TIP FOR SELECTED MODULI RATIOS
LOG OF MAXIMUM PRINCIPLE STRESS PER UNIT LOAD
10
1
End of 1/√r Singularity
Boundary of Super Element
Ea/E = 2
End of Singularity
Ea/E = 20
End of Singularity
Ea/E = 200
.01
.1
1.0
LOG OF DISTANCE FROM CRACK TIP IN ADHESIVE THICKNESSES

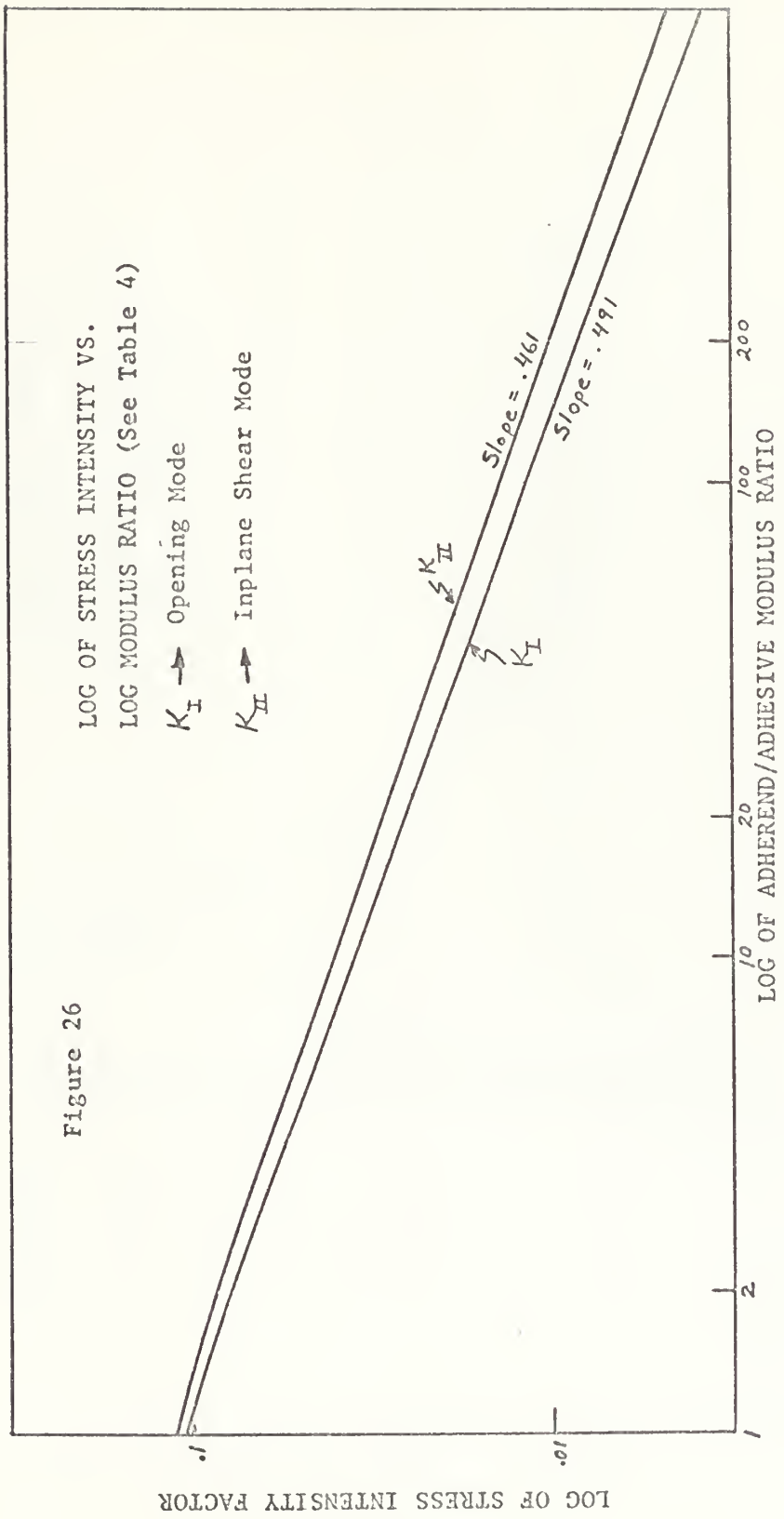
LOG OF STRESS INTENSITY VS.
LOG MODULUS RATIO (See Table 4)
K_I → Opening Mode
K_{II} → Inplane Shear Mode
Slope = .461
Slope = .491
K_{II}
K_I
LOG OF STRESS INTENSITY FACTOR
LOG OF ADHEREND/ADHESIVE MODULUS RATIO
.1
.01
1
2
10
20
100
200

Figure 26

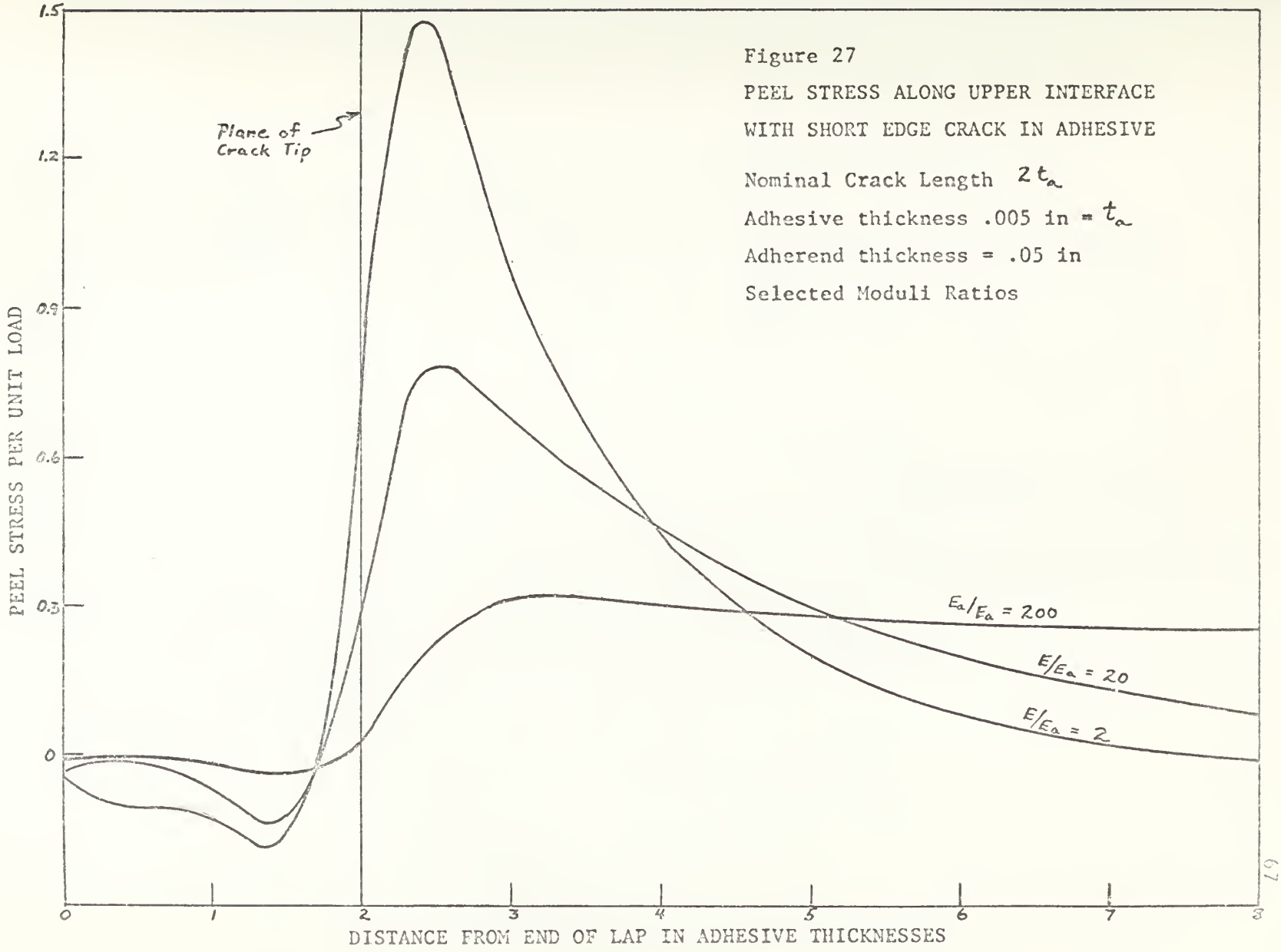

Figure 27

PEEL STRESS ALONG UPPER INTERFACE WITH SHORT EDGE CRACK IN ADHESIVE

Nominal Crack Length $2t_a$

Adhesive thickness .005 in = t_a

Adherend thickness = .05 in

Selected Moduli Ratios

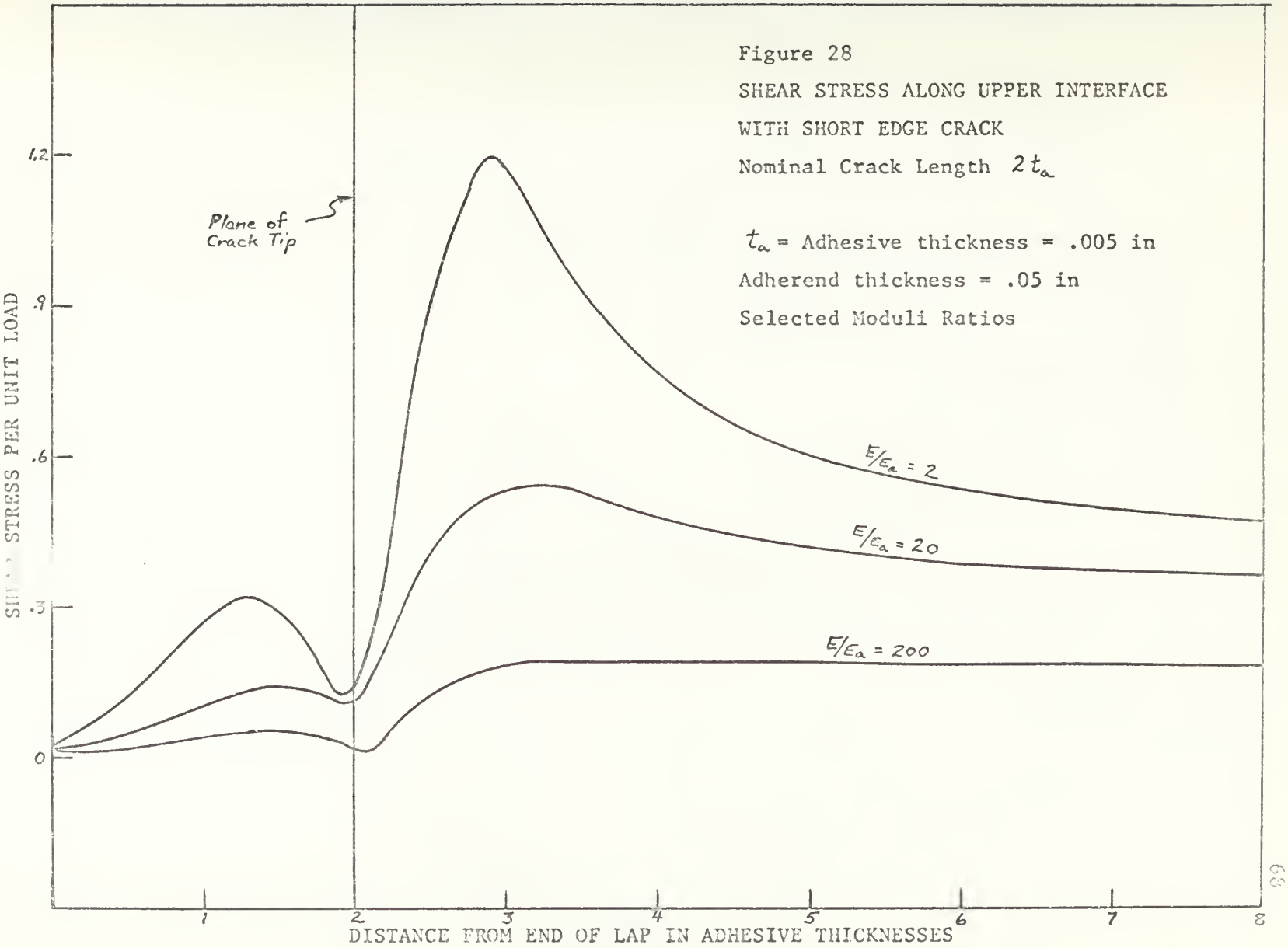
Figure 28
SHEAR STRESS ALONG UPPER INTERFACE
WITH SHORT EDGE CRACK
Nominal Crack Length $2t_a$
t_a = Adhesive thickness = .005 in
Adherend thickness = .05 in
Selected Moduli Ratios
Plane of Crack Tip
$E/E_a = 2$
$E/E_a = 20$
$E/E_a = 200$
1.2
.9
.6
.3
0
1
2
3
4
5
6
7
8
DISTANCE FROM END OF LAP IN ADHESIVE THICKNESSES

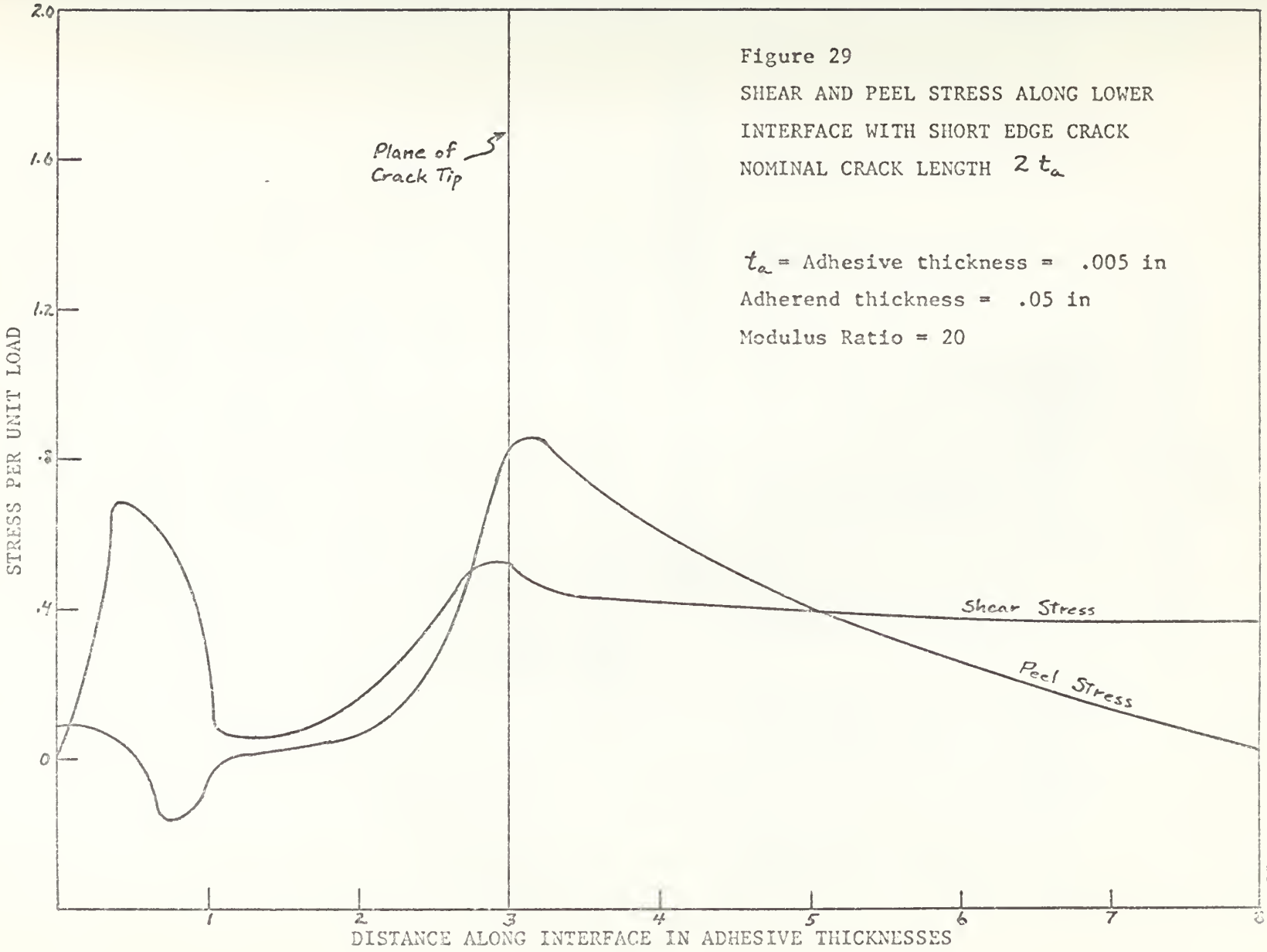

Figure 29

SHEAR AND PEEL STRESS ALONG LOWER INTERFACE WITH SHORT EDGE CRACK

NOMINAL CRACK LENGTH $2\,t_a$

t_a = Adhesive thickness = .005 in

Adherend thickness = .05 in

Modulus Ratio = 20

Table 1

Comparison to Goland Reissner Solution

Distance from end of lap (in)	Peel Stress σ_y			Shear Stress τ_{xy}		
		Current Solution			Current Solution	
	G-R	Midplane	Pt B	G-R	Midplane	Pt B
0.0005	0.839	0.832	1.137	0.599	0.547	0.735
0.0015	0.794	0.791	0.825	0.585	0.504	0.612
0.003	0.730	0.695	0.725	0.564	0.485	0.571
0.006	0.610	0.541	0.560	0.524	0.462	0.520
0.013	0.371	0.286	0.310	0.442	0.394	0.448
0.034	-0.055	-0.012	0.000	0.265	0.258	0.266
0.100	-0.084	-0.116	-0.111	0.054	0.076	0.077
0.200	0.006	0.043	0.046	0.005	0.001	-0.004

The following parameters were used in above solutions

Adherend - Aluminum ($E = 10^7$, $\nu = 0.33$)

Elastic Adhesive ($E = 500{,}000$, $\nu = 0.35$)

Adhesive thickness = 0.005 inch

Adherend thickness = 0.05 inch

Overlap length = 0.5 inch

Loading - 1 psi tension in adherend

Table 2

Comparison of Stress Intensity Factor k_I for Symmetric Loading with Existing Solutions [31]

Method of Evaluating k_I	Stress Intensity Factor, k_I Direct	Crack Opening
Pian,Tong,Luk [30]		
Mesh D.O.F.		
1 x 2 24	0.840	0.904
2 x 4 72	0.822	0.797
4 x 4 128	0.812	0.784
4 x 6 184	0.791	0.790
Five Node Symmetric Super Element [31]		
2 x 3 22	0.793	—
4 x 5 58	0.794	—
Nine Node General Super Element (Present Solution)		
6 x 8 130	0.793*	—
"Exact" Solution Bowie [33]	0.793	

*$k_{II} = 1.7 \times 10^{-5}$

Table 3

STIFFNESS MATRIX FOR NINE NODE GENERAL SUPER ELEMENT (18 X 18)

Note: Matrix is symmetric so only lower triangle is shown. Part 1 is columns 1-6, Part 2 is columns 7-12, and Part 3 is columns 13-18.

PART 1

0.6685E+00						
0.0	0.5966E+00					
0.2349E-01	0.8809E-01	0.3252E+00				
-0.5313E-01	-0.1196E+00	0.6209E-01	0.3249E+00			
-0.1687E+00	0.8303E-01	-0.1210E+00	0.7691E-01	0.5710E+00		
0.1459E+00	-0.1616E+00	-0.7351E-01	0.1380E-01	-0.1165E-01	0.5689E+00	
-0.9502E-01	0.2482E-01	-0.6528E-01	-0.1766E-01	-0.1024E+00	0.6236E-01	
0.6303E-01	-0.1779E-01	0.1516E-01	-0.3225E-01	-0.1546E+00	-0.2353E-01	
-0.9400E-01	0.1039E-01	-0.7393E-01	-0.4102E-01	-0.1609E+00	-0.1529E+00	
-0.5295E-02	0.6074E-03	-0.1007E-01	0.1141E-01	-0.2404E-01	-0.1451E+00	
-0.9400E-01	-0.1039E-01	-0.1978E-01	-0.2088E-01	-0.2777E-02	0.4531E-02	
0.5295E-02	0.6074E-03	-0.6995E-02	0.2428E-02	0.8306E-02	-0.3251E-02	
-0.9502E-01	-0.2482E-01	-0.2082E-01	-0.2641E-01	-0.5198E-02	-0.1930E-01	
-0.6303E-01	-0.1779E-01	-0.1271E-01	-0.2235E-01	-0.1539E-01	-0.2785E-01	
-0.1687E+00	-0.8303E-01	-0.1491E-01	-0.1711E-01	0.4875E-02	-0.2036E-01	
-0.1459E+00	-0.1616E+00	-0.6485E-01	-0.9991E-01	0.2036E-01	-0.1215E+00	
0.2349E-01	-0.8809E-01	-0.1294E-01	0.1723E-01	-0.1491E-01	0.6484E-01	
0.5313E-01	-0.1196E+00	-0.1723E-01	-0.7848E-01	0.1712E-01	-0.9991E-01	

PART 2

0.3047E+00						
-0.3014E-01	0.1321E+00					
0.2251E-01	0.7208E-01	0.3585E+00				
-0.7893E-01	-0.1191E-01	0.1075E+00	0.1414E+00			
-0.1281E-01	0.7961E-02	-0.1690E-01	0.4453E-02	0.3585E+00		
-0.7701E-02	0.1884E-01	-0.4453E-02	-0.1444E-01	-0.1075E+00	0.1414E+00	
-0.5711E-02	-0.1552E-02	-0.1281E-01	0.7702E-02	0.2251E-01	0.7893E-01	
0.1552E-02	-0.1528E-01	-0.7961E-02	0.1884E-01	-0.7208E-01	-0.1191E-01	
-0.5199E-02	0.1539E-01	-0.1777E-02	-0.8307E-02	-0.1609E+00	0.2403E-01	
0.1929E-01	-0.2785E-01	-0.4530E-02	-0.3252E-02	0.1529E+00	-0.1451E+00	
-0.2082E-01	0.1271E-01	-0.1978E-01	0.6995E-02	-0.7393E-01	0.1007E-01	
0.2641E-01	-0.2235E-01	0.2088E-01	0.2429E-02	0.4102E-01	0.1141E-01	

Table 3 Continued

	0.3047E+00					
	0.3014E-01	0.1321E+00				
PART 3	-0.1024E+00	0.1546E+00	0.5710E+00			
	-0.6236E-01	-0.2353E-01	0.1165E-01	0.5689E+00		
	-0.8528E-01	-0.1516E-01	-0.1210E+00	0.7351E-01	0.3252E+00	
	0.1766E-01	-0.3225E-01	-0.7691E-01	0.1380E-01	-0.8209E-01	0.3249E+00

Table 4

Stress Intensity Factors k_I and k_{II} for Selected Moduli Ratios

Adherend to Adhesive Modulus	Stress Intensity Factor	
	k_I	k_{II}
1	.1040	.1096
2	.0774	.0845
20	.0253	.0291
200	.0083	.0101

Geometry as shown in Figure I

Mesh arrangement as shown in Figure II

Total Degrees of Freedom = 1144

Total Number of Elements = 509

BIBLIOGRAPHY

1. Goland,M. and E. Reissner,"The Stresses in Cemented Joints ," *Journal of Applied Mechanics*, Vol. 11, No. 1, (1944), pp A17-A27.

2. Forest Products Laboratory, U.S. Department of Agriculture ,"Determination of Mechanical Properties for use in the Design of Bonded Joints," September 1963.

3. Cornell,R.W.,"Determination of Stresses in Cemented Lap Joints," *Journal of Applied Mechanics*, Vol. 20, No. 3, (1953), pp 355-364.

4. Wang, T.T., F.W. Ryan and H. Schonhorn,"Effect of Bonding Defects on Shear Strength in Tension of Lap Joints Having Brittle Adhesives," *Journal of Applied Polymer Science* , Vol. 16, (1972), pp 1901-1909.

5. Schijve,J.,"Some Elementary Calculations on the Secondary Bending in Simple Lap Joints," National Aerospace Laboratory , Amsterdam, Netherlands, Report No. NLR-TR-72036-U, (1972).

6. Chang,D.J. and R. Muki,"Stress Distribution in a Lap Joint Under Tension-Shear," *International Journal of Solids and Structures*, Vol. 10, (1974), pp 503-517.

7. Srinivas,S.,"Analysis of Bonded Joints," NASA Technical Note, Langley Research Center, Hampton, Va., NASA-TN -D-7855, (1975).

8. Desai, C.S. and J.F. Abel, *Introduction to the Finite Element Method*, VanNostrand Reinhold Company, New York , (1972).

9. Zienkiewicz, O.C. and Y.K. Cheung, *The Finite Element Method in Structural and Continuum Mechanics*, McGraw-Hill , London, (1967).

10. Wooley,G.R. and D.R. Carver,"Stress Concentration Factors for Bonded Lap Joints," *Journal of Aircraft*, Vol. 8, No. 10, (1971), pp 817-820.

11. Harrison,N.L. and W.J. Harrison,"Stresses in an Adhesive Layer," *Journal of Adhesion*, Vol. 3, (1972), pp 195-212.

12. Pirvics,J.,"Two Dimensional Displacement-Stress Distributions in Adhesive Bonded Composite Structures," *Journal of Adhesion* , Vol. 6, (1974), pp 207-228.

13. Adams,R.D. and N.A. Peppiatt,"Stress Analysis of Adhesive Bonded Lap Joints," *Journal of Strain Analysis*, Vol. 9, No. 3, (1974), pp 185-196.

14. Forest Products Laboratory, U.S. Department of Agriculture ,"Mechanics of Adhesive Bonding Lap-Type Joints: Survey and Review," Report No. ML-TDR-64-298, (1964).

15. Douglas Aircraft Company, Inc., Santa Monica, California ,"Photostress Investigation of Bonded Lap Joints, Part II ," by K.F. Hahn, Research Report SM 40001 (1961).

16. Forest Products Laboratory, U.S. Department of Agriculture ,"Photoelastic Analysis of Shear Stress Distribution in Adhesive -Bonded Lap Joints," by D. Kutscha, Report TP-122 (1962).

17. Demarkles,L.R.,"Investigation o the use of a Rubber Analog in the Study of Stress Distribution in Riveted and Cemented Joints," NASA Technical Note 3413 (1955).

18. Adams,R.D., S.H. Chambers, P.J.A. Del Strother, and N.A. Peppiatt,"Rubber Model for Adhesive Lap Joints," *Journal of Strain Analysis*, Vol. 8, No. 1, (1973), pp 52-57.

19. Dukes,W.A. and R.W. Bryant,"The Effect of Adhesive Thickness on Joint Strength," *Journal of Adhesion*, Vol. 1, (1969) , pp 48-53.

20. Grimes,G.C.,"Stress Distribution in Adhesive Bonded Lap Joints," SAE Paper 710107, (1971).

21. Pian,T.H.H. and Pin Tong," Basis of Finite Element Methods for Solid Continua," *International Journal for Numericasl Methods in Engineering*, Vol. 1, (1969), pp 3-28.

22. Pian,T.H.H.,"Derivation of Element Stiffness Matrices by Assumed Stress Distributions," *AIAA Journal*, Vol. 2, No. 7, (1964), pp 1333-1336.

23. Luk,C.H.," Assumed Stress Hybrid Finite Element Method for Fracture Mechanics and Elastic-Plastic Analysis," Air Force Office of Scientific Research, U.S. Air Force, Report No. AFOSR-TR-73-0493, (1972).

24. Mostovoy,S. and E.J. Ripling,"Fracture Characteristics of Adhesive Joints," Final Report 1 January 1973- 31 January 1974, Naval Air Systems Command Contract Report AD-A001-335 , (1974).

25. Jemian,W.A. and M.B. Ventrice,"The Fracture Toughness of Adhesive Bonded Joints," *Journal of Adhesion*, Vol. 1, (1969), pp 190-207.

26. Wilson,W.K.,"Stress Intensity Factors for Deep Cracks in Bending and Compact Tension Specimen,"*Engineering Fracture Mechanics*, Vol. 2, (1970), pp169-171.

27. Tratina,G.G.,"Combined Mode Crack Extension in Adhesive Joints," *Journal of Composite Materials*, Vol. 6, (1972) , pp 371-385.

28. Anderson,G.P., K.L. deVries and M.L. Williams," Finite Element in Adhesion Analysis," *International Journal of Fracture*, Vol. 9, (1973), pp 421-436.

29. Williams,M.L.,"The Relation o Continuum Mechanicss to Adhesive Fracture," *Journal of Adhesion*, Vol. 4, (1972) , pp 307-332.

30. Pian,T.H.H., P. Tong and C.H. Luk,"Elastic Crack Analysis by a Finite Element Hybrid Method," paper presented at *3rd Conference on Matrix Methods in Structural Mechanics* , Wright-Patterson Air Force Base, Ohio (October 19-21,1971).

31. Lasry,S.J.,"Derivation of Crack Element-Stifness Matrix by the Complex Variable Approach," Air Orce Office o Scientific Research, U.S. Air Force, Report No. AFORS-TR-73-1602 , (1973).

32. Tong,P.,T.H.H. Pian and S.J. Lasry,"A Hybrid-Element Approach to Crack Problems in Plane Elasticity,"*International Journal or Numerical Methods in Engineering*, Vol. 7, (1973) , pp 297-308.

33. Bowie,O.L.,"Rectangular Tensile Sheets with Symmetric Edge Cracks," *Journal of Applied Mechanics*, Vol. 31, (1964) , pp 208-212.

34. Erdogan,F.,*Journal of Applied Mechanics*, Vol. 30 , (1963), pp 232.

35. Tong,P.,and T.H.H. Pian,"The Convergence of Finite Element Method in Solving Linear Elastic Problems," *International Journal of Solids and Structures*, Vol. 3, (1967), pp 865-879.

36. Cherry,B.W. and N.L. Harrison,"The Optimum Profile for a Lap Joint," *Journal of Adhesion*, Vol. 2, (1970), pp 125-128.

37. Muskhelishvili,N.I.,"Some Basic Problems in the Mathematical Theory of Elasticity, "(J.R.M. Radok Trans.),Noordhoff, Groningen,Holland,(1953).

Thesis 164322
C4497 Christensen
A finite element analysis of a single lap shear adhesive joint with and without an edge crack.